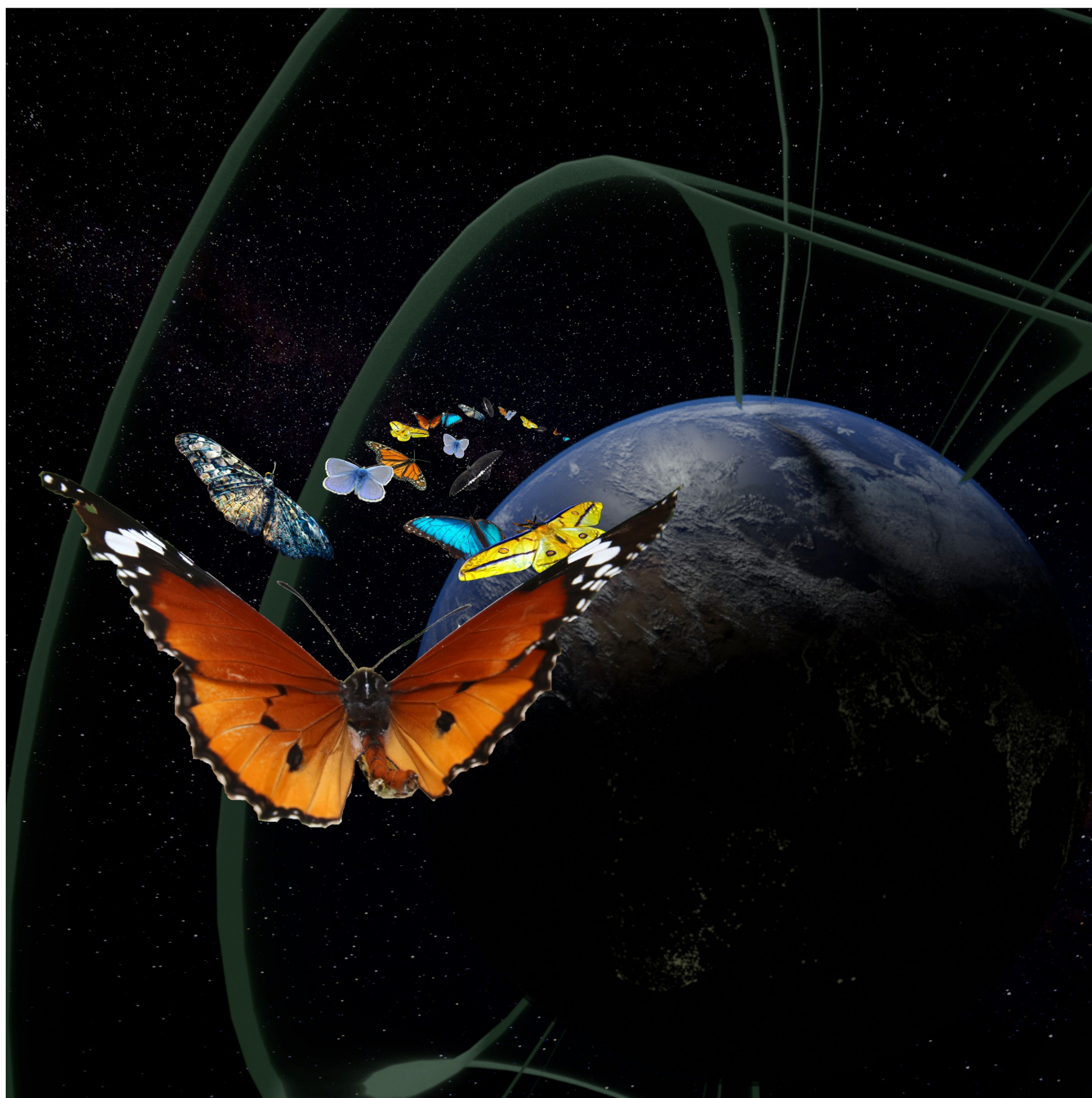


Special  
Issue

# From the $\{\text{Fe}^{\text{III}}_2\text{Ln}_2\}$ Butterfly's Perspective: the Magnetic Benefits and Challenges of Cooperativity within 3d–4f Based Coordination Clusters

Yan Peng,<sup>\*,[a, b, c]</sup> Hagen Kaemmerer,<sup>[a, d]</sup> and Annie K. Powell<sup>\*,[a, b, d]</sup>

**Abstract:** In this Review we discuss the tuning handles which can be used to steer the magnetic properties of Fe<sup>III</sup>-4f “butterfly” compounds. The majority of presented compounds were produced in the context of project A3 “Di- to tetranuclear compounds incorporating highly anisotropic paramagnetic metal ions” within the SFB/TRR88 “3MET”. These contain {Fe<sup>III</sup><sub>2</sub>Ln<sub>2</sub>} cores encapsulated in ligand shells which are easy to tune in a “test-bed” system. We identify the following advantages and variables in such systems: (i) the complexes are structurally simple usually with one crystallographically independent Fe<sup>III</sup> and Ln<sup>III</sup>, respectively. This simplifies theory and analysis; (ii) choosing Fe allows <sup>57</sup>Fe Mössbauer spectroscopy to be used as an additional technique which can give information about oxidation levels and spin states, local moments at the iron nuclei and spin-relaxation and, more importantly, about the anisotropy not only of the studied isotope, but also of elements interacting

with this isotope; (iii) isostructural analogues with all the available (i.e. not Pm) 4f ions can be synthesised, enabling a systematic survey of the influence of the 4f ion on the electronic structure; (iv) this cluster type is obtained by reacting [Fe<sup>III</sup><sub>3</sub>O(O<sub>2</sub>CR)<sub>6</sub>(L)<sub>3</sub>](X) (X=anion, L=solvent such as H<sub>2</sub>O, py) with an ethanolamine-based ligand L' and lanthanide salts. This allows to study analogues of [Fe<sup>III</sup><sub>2</sub>Ln<sub>2</sub>(μ<sub>3</sub>-OH)<sub>2</sub>(L')<sub>2</sub>(O<sub>2</sub>CR)<sub>6</sub>] using the appropriate iron trinuclear starting materials. (v) the organic main ligand can be readily functionalised, facilitating a systematic investigation of the effect of organic substituents on the ligands on the magnetic properties of the complexes. We describe and discuss 34 {M<sup>III</sup><sub>2</sub>Ln<sub>2</sub>} (M=Fe or in one case Al) butterfly compounds which have been reported up to 2020. The analysis of these gives perspectives for designing new SMM systems with specific electronic and magnetic signatures

## 1. Introduction

It is clear that factors such as the ligand field and the coordination geometry of the individual ions as well as the strength of the magnetic interaction can influence the SMM behaviour.<sup>[1]</sup> It is still a significant challenge to establish useful guidelines for constructing 3d–4f based clusters exhibiting enhanced or unusual SMM properties. Therefore, the synthesis of series of 3d–4f coordination clusters with a given core motif should provide a test-bed for examining the influence of various tuning handles on the system. Among the coordination clusters containing four metal centres, possible arrangements

include cubane-like (Figure 1a),<sup>[2]</sup> ring-shaped (Figure 1b),<sup>[3]</sup> propeller-shaped (Figure 1c),<sup>[4]</sup> co-planar arrangements<sup>[5]</sup> (Figure 1d), and so on.<sup>[6]</sup>

The butterfly topology is one of the most interesting motifs from the viewpoint of a magneto-structural correlation study. This motif is well-known for pure 3d<sup>[7]</sup> and pure 4f systems.<sup>[8]</sup> And in terms of general arrangement of the metal ions for 3d–4f butterflies, we are usually dealing with the generic {M<sup>III</sup><sub>2</sub>Ln<sup>III</sup><sub>2</sub>}, where M is a transition metal ion, or possibly a main group diamagnetic metal ion, and Ln is a rare earth ion, defined as metal ions from group 3 (Sc, Y, La) and the 4f ions of the lanthanide series.<sup>[9]</sup> Such coordination clusters can have one of two arrangements.

Type I (see Scheme 1) has the 4f ions occupying the wingtip positions of the butterfly. When the Ln ions are in the wingtips and the Fe in the body, there are Fe–Ln coupling, Ln single ion properties as well as the strong Fe–Fe coupling to consider. This gives 3 different parameters, as well as contributions from dipolar coupling. When the central M is either diamagnetic or else not coupled to any significant extent to the 4f ion we might expect the 4f single ion properties to dominate the magnetism. When the 3d–4f and 3d–3d coupling parameters are significant, the system has to be treated as a cooperative entity. In addition, the role of the dipolar coupling and the relative anisotropies of the two types of ions must be considered. For the Type II case, if for example the Fe<sup>III</sup> ions are at the wingtip positions, this effectively deletes the Fe<sup>III</sup>–Fe<sup>III</sup> interaction, but presumably keeping the Fe<sup>III</sup>–Dy interaction as well as the single ion properties of the Ln.

Here we can expect the lanthanide single ion properties to dominate. The most celebrated examples of the Type II butterflies have been for M<sup>III</sup>=Cr<sup>III</sup> and Co<sup>III</sup> with Dy<sup>III</sup> in the body positions, aminoalcohol ligands and bridging carboxylates from the Murray group.<sup>[10]</sup>


We have deliberately chosen a “test-bed” system based on {M<sub>2</sub>Ln<sub>2</sub>} butterfly cores which can show good overall SMM


[a] Dr. Y. Peng, H. Kaemmerer, Prof. A. K. Powell  
Institute of Inorganic Chemistry  
Karlsruhe Institute of Technology  
Engesserstr. 15, 76131 Karlsruhe (Germany)  
E-mail: yan.peng@kit.edu  
annie.powell@kit.edu

[b] Dr. Y. Peng, Prof. A. K. Powell  
Institute for Nanotechnology (INT)  
Karlsruhe Institute of Technology  
Hermann-von-Helmholtz-Platz 1, 76344 Eggenstein-Leopoldshafen (Germany)

[c] Dr. Y. Peng  
School of Chemistry and Chemical Engineering  
Jiangxi University of Science and Technology  
Ganzhou 341000 (P.R. China)

[d] H. Kaemmerer, Prof. A. K. Powell  
Institute for Quantum Materials and Technologies (IQMT)  
Karlsruhe Institute of Technology  
Hermann-von-Helmholtz-Platz 1, 76344 Eggenstein-Leopoldshafen (Germany)

 This manuscript is part of a Special Issue “Cooperative effects in heterometallic complexes”.

 © 2021 The Authors. Chemistry - A European Journal published by Wiley-VCH GmbH. This is an open access article under the terms of the Creative Commons Attribution Non-Commercial NoDerivs License, which permits use and distribution in any medium, provided the original work is properly cited, the use is non-commercial and no modifications or adaptations are made.

behaviour. The most common 3d–4f butterflies involve Fe<sup>III</sup> as the 3d ion. The other examples of 3d–4f butterflies were recently reviewed by us.<sup>[9]</sup> We will discuss how to quantify “good” in this context in the next section. In order to truly test this “test-bed” we selected {M<sub>2</sub>Ln<sub>2</sub>} where M=high spin Fe<sup>III</sup>. There are two main reasons for this choice.

1. These systems generally show slow relaxation of the magnetisation which is taken as an indication of some level of SMM behaviour (again, see next section for an in depth discussion of this) but none of these systems counts as particularly “good” in SMM terms. This is the reason why they have been chosen: any small enhancement or worsening of the desired SMM parameters is easily picked up in an analysis of the ac behaviour.
2. By using M=Fe<sup>III</sup> we have the additional handle of <sup>57</sup>Fe Mössbauer spectroscopy, which has been shown to be a very useful adjunct operating on a different timescale from that of SQUID magnetometry in the ac mode. Furthermore, we can apply much larger static fields using this technique, which taken together allows us to examine relaxation processes on both faster timescales and with increased

understanding of the dynamics of the magnetisation relaxation.

On surveying what at a first glance seems to provide an extensive test-bed for exploring the tuning and fine-tuning parameters for “butterfly” 3d/4f Single Molecule Magnets (SMMs) it quickly becomes apparent that any perspective here disappears into a perplexing fog of confusion. The perplexment is a result of the fact that several research groups have explored these butterflies using a variety of approaches and benchmarks - in other words, there no consistent protocols for measuring and evaluating have been applied across the board.<sup>[9]</sup> In the light of this, we decided to screen our results on a particular {Fe<sup>III</sup><sub>2</sub>Ln<sub>2</sub>} butterfly system, reanalysing systems where necessary, in order to come-up with a consistent picture of the state-of-the-art from the {Fe<sup>III</sup><sub>2</sub>Ln<sub>2</sub>} butterfly’s perspective.

In this review, alongside our own results on this system we present other {Fe<sup>III</sup><sub>2</sub>Ln<sub>2</sub>} butterflies from the literature up to 2020 where slow relaxation of the magnetisation hinting at SMM properties has been reported.

## 2. Experimental Methods and Benchmarks

### 2.1. Single-crystal X-ray structure

To analyse the magnetic behaviour a first requirement is to determine the molecular structure using X-ray diffraction. For an isostructural series of compounds it can suffice to determine the structural details for one member of the series and then check the unit cells and powder X-ray diffraction patterns of the other members. However, if detailed magneto-structural correlations are the aim, then it is necessary to collect metric details for all members of the family. In addition to the crystal structure, the material is characterised using standard analytical techniques. Elemental analysis is vital since crystalline samples can lose solvent molecules such as methanol or acetonitrile which often are replaced by water taken up from the atmosphere.

### 2.2. Magnetic properties

Bulk susceptibility studies are generally performed using a SQUID magnetometer. There are no set rules on how best to perform these measurements with different groups preferring different sample preparation and applying different benchmarks. Several pitfalls need to be avoided. (a) It is important to ensure that samples do not align with the applied field, usually this is prevented by constraining the sample. (b) A consensus on defining a blocking temperature is beginning to emerge when looking at ac susceptibility data. The out-of-phase signals can provide a benchmark when maxima are observed. Since the data measured at 1000 Hz can be taken as reliable for most SQUID magnetometers, the position of this maximum is suggested as the benchmark for providing the blocking temperature. (c) For hysteresis measurements care needs to be taken in terms of the sweep rate of the measurement. (d) Small

Yan Peng obtained his PhD from the Karlsruhe Institute of Technology in 2015 under the supervision of Prof. Annie K. Powell. His research focus is magnetic characterisation of coordination clusters. He took on the position of associate professor at Jiangxi University of Science and Technology in 2020.



Hagen Kaemmerer is currently pursuing his PhD focussing on cyclic 3d/4f coordination clusters at Karlsruhe Institute of Technology under the guidance of Prof. Annie K. Powell.



Annie Powell gained her PhD degree from the University of Manchester in 1985 and subsequently undertook post-doctoral research at the University of Freiburg, Germany. In 1999 she took up the Chair of Supramolecular Chemistry at the University of Karlsruhe, Germany. The main focus of her current research is using coordination chemistry principles in exploring the synthesis, properties and descriptions of nanoscaled structures.





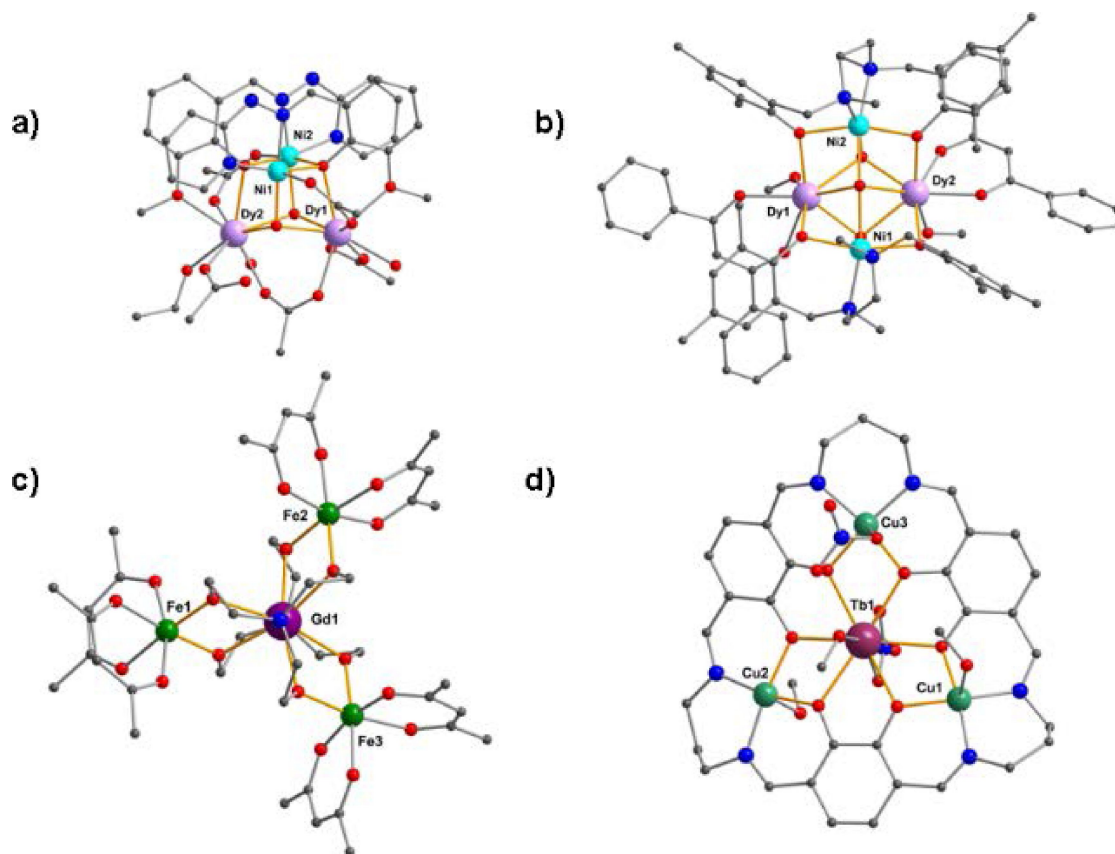
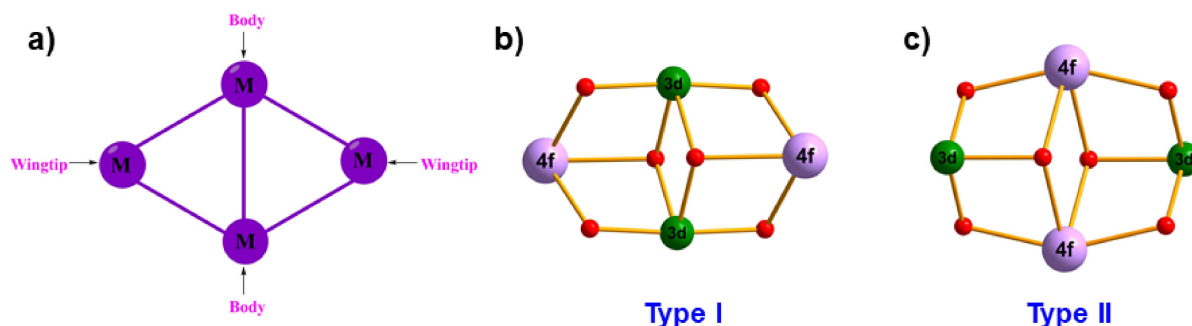


**Figure 1.** (a) Molecular structure of cubane-like  $\{\text{Ni}^{\text{II}}_2\text{Dy}_2\}$  complex; (b) molecular structure of ring-like  $\{\text{Ni}^{\text{II}}_2\text{Dy}_2\}$  complex; (c) molecular structure of propeller-like  $\{\text{Fe}^{\text{III}}_3\text{Gd}\}$  complex; (d) molecular structure of co-planar  $\{\text{Cu}^{\text{II}}_3\text{Tb}\}$  complex.



**Scheme 1.** The definition of the body and wingtip in butterfly  $\text{M}_4$  cores (a); Ball and stick representation of the metal-oxo ( $3\text{d}_2\text{Ln}_2\text{O}_6$ ) core of a defective dicubane or butterfly structure (b and c).

amounts of paramagnetic “impurities” (these can be a result of uncompensated surface spins) need to be handled properly.

Single-crystal experiments can be very informative. Usually large enough single crystals are not available for a standard SQUID magnetometer, but arrays of single crystals are used for micro-SQUID studies and help in identifying easy axes of magnetisation. Single-crystal torque magnetometry can also be informative.

### 2.3. Other methods

Various spectroscopies, including some with applied magnetic fields, can add further insights into the magnetic and electronic properties as well as helping to explore relaxation pathways, including phonon-mediated ones. For the  $\{\text{Fe}^{\text{III}}_2\text{Ln}_2\}$  butterflies  $^{57}\text{Fe}$  Mössbauer spectroscopy gives extra insights on how the presence of 4f ions affects the local environment of the  $\text{Fe}^{\text{III}}$  ions.



## 2.4. Theory

Calculations aimed towards unravelling magneto-structural correlations and understanding the extent and nature of magnetic coupling become very challenging for open shell systems with large Hilbert space dimensions. Great progress has been made in recent years on rising to these challenges, but there is no real consensus on the “best” way to perform such calculations.

Probably the most rigorous approach is to perform ab initio calculations on the so called “Complete Active Space Self-Consistent Field” abbreviated to CASSCF. This requires the application of chemical insights into the system in order to map out the parameters for the active space. This active space contains the electrons and orbitals needed to describe the electronic structure of the molecule. This, in turn, requires input from, for example, Density Functional Theory (DFT) to calculate the orbitals, usually via the Broken Symmetry approach, which breaks spin and often also spatial symmetry. This can be especially challenging for ions with large anisotropies.<sup>[11]</sup> Further challenges are dealing with the very different natures of the 3d and 4f ions when defining the active space.

## 2.5. Scope of the perspective presented

As mentioned above, combining 3d and 4f ions can lead to systems where the overall “performance” of SMMs can be optimised. As the term suggests, optimisation means arriving at the best compromise for a set of “tuning handles” in order to get the best overall performance of the system.<sup>[12]</sup> This, in turn, implies that no single parameter will be the “biggest or best”. It has been demonstrated profusely, for example, that aiming for the “biggest spin” or the largest anisotropy barrier does not tick all the boxes in terms of what is required for a “performant SMM”. For example, the largest spin for a 3d molecule incorporating anisotropic Mn(III) completely failed to produce an SMM system<sup>[13]</sup> and the appealingly high barriers for the highly axial sandwich compound,  $[(\eta^5\text{-Cp}^*)\text{Dy}(\eta^5\text{-Cp}^{\text{Pr}5})][\text{B}(\text{C}_6\text{F}_5)_4]$ , ( $\text{Cp}^{\text{Pr}5}$  = penta-iso-propylcyclopentadienyl and  $\text{Cp}^*$  = pentamethylcyclopentadienyl), which currently has the largest reported 4f anisotropy barrier  $U_{\text{eff}} = 1541 \text{ cm}^{-1}$  for the reversal of magnetisation<sup>[14]</sup> is found for a system which is air sensitive, thus not meeting the requirement of a robust molecule.

To summarise, finding the optimum set of parameters takes the following points into consideration:

1. Barrier height is not a deciding factor, rather quenching QTM is important. This requires finding systems where the QTM probability is minimised.
2. QTM is not the only issue. Other relaxation pathways are available and it has recently been acknowledged that one of the most important relaxation pathways may be via the lattice through spin-phonon coupling.
3. The local electronic structures of the component ions will be relevant as will the nature and extent of magnetic coupling between these ions.

4. Studies where either the 3d or 4f ions are varied can give great insights into how the magnetic behaviour may be tuned.
5. Related to this, studies where the paramagnetic contribution of either the 3d or the 4f ions is completely “knocked-out” by virtual (theory) or real substitution (practice) by diamagnetic ions, helps to identify the cooperativity within the 3d–4f system.
6. There is still no real quantification of how much small structural changes in what seem to be isostructural compounds affect the magnetic behaviour. Whilst routines such as a SHAPE analysis provide information regarding the coordination geometry of individual 3d and 4f ions, a more careful analysis of the structural metrics can reveal situations where zero-field splitting parameters and optimised Ising anisotropies become more or less optimised.
7. Related to this is the effect of small changes to the electronic structure arising from variations in the coordinating ligands.

## 2.6. Geometries in this review

In this review, the idealised geometries of the metal ions in each of the structurally characterised complexes described were determined using the program SHAPE.<sup>[15]</sup> The ‘continuous shape measure’ (CSHM) accompanying each geometry in Table 1 is a measure of how far from that idealised polyhedron the geometry is (with zero being ideal). The organic main ligands and co-ligands are also listed in Table 1. The closest coordination geometries of iron ions and the three closest geometries of the lanthanide ions in the reported  $\{\text{Fe}^{\text{III}}_2\text{Ln}_2\}$  butterfly systems are given in Table 1. The relevant coordination polyhedra are shown in Figure 2 which correspond to the six-, eight-, and nine- vertex polyhedral for the lanthanide ions.<sup>[16]</sup> All six coordinate 3d ions are close to octahedral (OC-6) coordination geometry. All the eight coordinate 4f ions are close to triangular dodecahedron (TDD-8) and all the nine coordinate 4f ions are close to capped square antiprismatic coordination geometry (CSAPR-9) except in  $[\text{NHEt}_3]_2[\text{Fe}^{\text{III}}_2\text{Gd}^{\text{III}}_2(\text{O}_2\text{Ph})_4(\text{thme})_2(\text{NO}_3)_4]$ , in which the nine coordinate 4f ions are close to muffin geometry (MFF-9). Since all

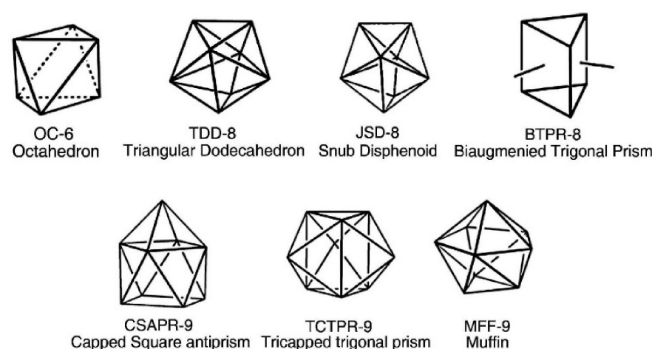


**Figure 2.** The six-, eight- and nine-coordinate geometries adopted by the metal ions in the reviewed complexes.

**Table 1.** Structural and magnetic features of reported Fe<sup>III</sup>-4f butterfly coordination clusters. The substitution at the *para*- or *meta*-positions of the benzoate ring is indicated by the first named group, for example *p*-Me indicates a methyl substituent in the *para*-position.

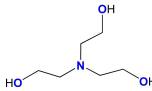
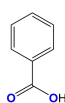
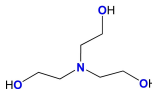
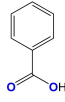
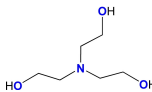
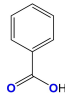
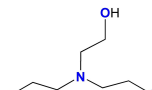
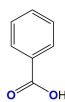
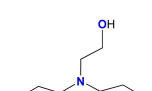
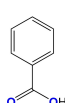
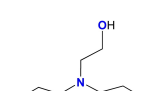
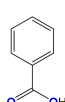
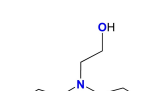
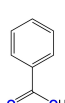
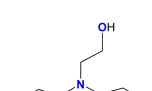
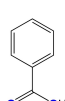
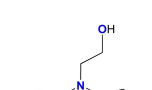
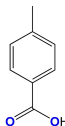
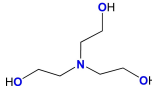
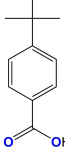
	Space group	$J_{Fe-Fe}$ [cm <sup>-1</sup> ]	Fe <sup>III</sup>	Ln <sup>III</sup>	Ligands	co-Ligands	Ref.
[Fe <sup>III</sup> <sub>2</sub> Ho <sub>2</sub> (OH) <sub>2</sub> (teaH) <sub>2</sub> ( <i>p</i> -H-PhCO <sub>2</sub> ) <sub>4</sub> (NO <sub>3</sub> ) <sub>2</sub> ] <b>1</b>	<i>P</i> -1	-5.69	(1.02)	(1.05) TCTPR-9 (1.37) MFF-9 (1.73)	teaH <sub>3</sub> 		[17]
[Fe <sup>III</sup> <sub>2</sub> Dy <sub>2</sub> (OH) <sub>2</sub> (teaH) <sub>2</sub> ( <i>p</i> -H-PhCO <sub>2</sub> ) <sub>6</sub> ] <b>3</b>	<i>C</i> 2/ <i>c</i>	-1.97	(0.73)	(1.55) CSAPR-9 (1.07) TCTPR-9 (1.34)	teaH <sub>3</sub> 		[18]
[Fe <sup>III</sup> <sub>2</sub> Ce <sub>2</sub> (OH) <sub>2</sub> (teaH) <sub>2</sub> ( <i>p</i> -H-PhCO <sub>2</sub> ) <sub>6</sub> ] <b>4</b>	<i>C</i> 2/ <i>c</i>	-5.22	(0.65)	(2.01) CSAPR-9 (1.37) TCTPR-9 (1.84)	teaH <sub>3</sub> 		[18b]
[Fe <sup>III</sup> <sub>2</sub> Gd <sub>2</sub> (OH) <sub>2</sub> (teaH) <sub>2</sub> ( <i>p</i> -H-PhCO <sub>2</sub> ) <sub>6</sub> ] <b>9</b>	<i>C</i> 2/ <i>c</i>	-5.44	(0.72)	(1.75) CSAPR-9 (1.12) TCTPR-9 (1.49)	teaH <sub>3</sub> 		[18b]
[Fe <sup>III</sup> <sub>2</sub> Tb <sub>2</sub> (OH) <sub>2</sub> (teaH) <sub>2</sub> ( <i>p</i> -H-PhCO <sub>2</sub> ) <sub>6</sub> ] <b>2</b>	<i>C</i> 2/ <i>c</i>	-5.0	(0.69)	(1.61) CSAPR-9 (1.05) TCTPR-9 (1.34)	teaH <sub>3</sub> 		[18b]
[Fe <sup>III</sup> <sub>2</sub> Ho <sub>2</sub> (OH) <sub>2</sub> (teaH) <sub>2</sub> ( <i>p</i> -H-PhCO <sub>2</sub> ) <sub>6</sub> ] <b>10</b>	<i>C</i> 2/ <i>c</i>	-5.03	(0.72)	(1.57) CSAPR-9 (1.11) TCTPR-9 (1.35)	teaH <sub>3</sub> 		[18b]
[Fe <sup>III</sup> <sub>2</sub> Er <sub>2</sub> (OH) <sub>2</sub> (teaH) <sub>2</sub> ( <i>p</i> -H-PhCO <sub>2</sub> ) <sub>6</sub> ] <b>11</b>	<i>C</i> 2/ <i>c</i>	-5.44	(0.76)	(1.53) CSAPR-9 (1.05) TCTPR-9 (1.30)	teaH <sub>3</sub> 		[18b]
[Fe <sup>III</sup> <sub>2</sub> Y <sub>2</sub> (OH) <sub>2</sub> (teaH) <sub>2</sub> ( <i>p</i> -H-PhCO <sub>2</sub> ) <sub>6</sub> ] <b>14</b>	<i>C</i> 2/ <i>c</i>	-5.49	(0.77)	(1.56) CSAPR-9 (1.08) TCTPR-9 (1.34)	teaH <sub>3</sub> 		[18b]
[Fe <sup>III</sup> <sub>2</sub> Dy <sub>2</sub> (OH) <sub>2</sub> (teaH) <sub>2</sub> ( <i>p</i> -Me-PhCO <sub>2</sub> ) <sub>6</sub> ] <b>15</b>	<i>P</i> -1	-5.74	(0.88)	(1.72) CSAPR-9 (1.19) TCTPR-9 (1.32)	teaH <sub>3</sub> 		[18a, 19]
[Fe <sup>III</sup> <sub>2</sub> Dy <sub>2</sub> (OH) <sub>2</sub> (teaH) <sub>2</sub> ( <i>p</i> - <sup>t</sup> Bu-PhCO <sub>2</sub> ) <sub>6</sub> ] <b>16</b>	<i>P</i> 2 <sub>1</sub> / <i>c</i>	-5.61	(0.75)	(1.65) CSAPR-9 (1.07) TCTPR-9 (1.27)	teaH <sub>3</sub> 		[18a]

Table 1. continued

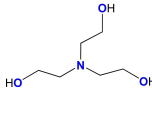
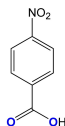
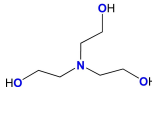
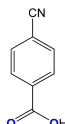
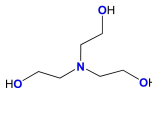
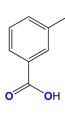
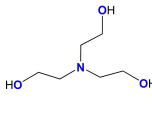
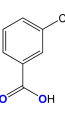
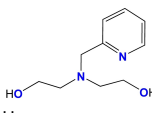
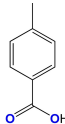
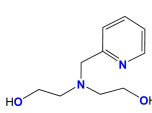
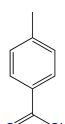
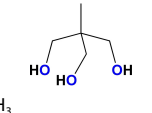
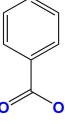
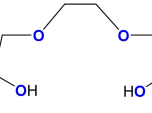
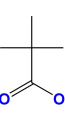
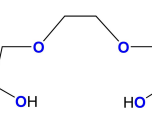
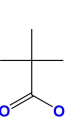
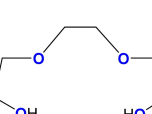
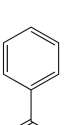
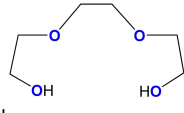
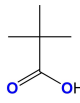
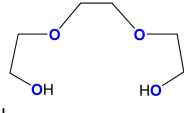
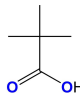
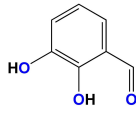
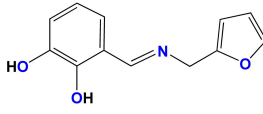
	Space group	$J_{\text{Fe-Fe}}$ [ $\text{cm}^{-1}$ ]	$\text{Fe}^{\text{III}}$	$\text{Ln}^{\text{III}}$	Ligands	co-Ligands	Ref.
$[\text{Fe}^{\text{III}}_2\text{Dy}_2(\text{OH})_2(\text{teaH})_2(p\text{-NO}_2\text{-PhCO}_2)_6]$ <b>17</b>	$P-1$	−5.78	OC-6 (0.92)	JCSAPR-9 (1.69) CSAPR-9 (1.00) TCTPR-9 (1.20)			[18a]
$[\text{Fe}^{\text{III}}_2\text{Dy}_2(\text{OH})_2(\text{teaH})_2(p\text{-CN-PhCO}_2)_6]$ <b>18</b>	$P2_1/c$	−5.23	OC-6 (0.83)	JCSAPR-9 (1.70) CSAPR-9 (1.13) TCTPR-9 (1.24)			[19]
$[\text{Fe}^{\text{III}}_2\text{Dy}_2(\text{OH})_2(\text{teaH})_2(m\text{e-Me-PhCO}_2)_6]$ <b>15a</b>	$P2_1/c$	−5.43	OC-6 (0.79)	JCSAPR-9 (1.65) CSAPR-9 (1.00) TCTPR-9 (1.33)			[19]
$[\text{Fe}^{\text{III}}_2\text{Dy}_2(\text{OH})_2(\text{teaH})_2(m\text{e-CN-PhCO}_2)_6]$ <b>18a</b>	$P-1$	−5.31	OC-6 (0.69)	JCSAPR-9 (1.69) CSAPR-9 (0.89) TCTPR-9 (1.08)			[19]
$[\text{Fe}^{\text{III}}_2\text{Dy}_2(\text{OH})_2(\text{pmide})_2(p\text{-Me-PhCO}_2)_6] \cdot 2\text{MeCN}$ <b>19</b>	$C2/c$	−5.28	OC-6 (0.80)	JCSAPR-9 (1.66) CSAPR-9 (1.01) TCTPR-9 (1.22)			[20]
$[\text{Fe}^{\text{III}}_2\text{Er}_2(\text{OH})_2(\text{pmide})_2(p\text{-Me-PhCO}_2)_6] \cdot 2\text{MeCN}$ <b>19a</b>	$C2/c$	−7.72	OC-6 (0.69)	JCSAPR-9 (1.50) CSAPR-9 (0.84) MFF-9 (1.27)			[21]
$[\text{NHEt}_3]_2[\text{Fe}^{\text{III}}_2\text{Gd}_2(\text{O}_2\text{Ph})_4(\text{thme})_2(\text{NO}_3)_4]$ <b>22</b>	$P2_1/n$	−3.17	OC-6 (0.29)	CSAPR-9 (2.82) TCTPR-9 (3.64) MFF-9 (2.23)			[22]
$[\text{Fe}^{\text{III}}_2\text{Dy}_2(\text{OH})_2(\text{teg})_2(\text{N}_3)_2(\text{piv})_4]$ <b>24</b>	$Pbca$	−	OC-6 (0.25)	TDD-8 (1.24) BTPR-8 (2.52) JSD-8 (2.63)			[23]
$[\text{Fe}^{\text{III}}_2\text{Y}^{\text{III}}_2(\text{OH})_2(\text{teg})_2(\text{N}_3)_2(\text{piv})_4]$ <b>23</b>	$Pbca$	−	OC-6 (0.27)	TDD-8 (1.21) BTPR-8 (2.54) JSD-8 (2.58)			[23]
$[\text{Fe}^{\text{III}}_2\text{Dy}^{\text{III}}_2(\text{OH})_2(\text{teg})_2(\text{N}_3)_2(\text{PhCO}_2)_4]$ <b>30</b>	$P-1$	−	OC-6 (0.29)	TDD-8 (1.30) BTPR-8 (2.40) JSD-8 (2.67)			[24]



Table 1. continued							
	Space group	$J_{Fe-Fe}$ [cm <sup>-1</sup> ]	Fe <sup>III</sup>	Ln <sup>III</sup>	Ligands	co-Ligands	Ref.
[Fe <sup>III</sup> <sub>2</sub> Dy <sup>III</sup> (MeO) <sub>2</sub> (teg) <sub>2</sub> (NO <sub>3</sub> ) <sub>2</sub> (piv) <sub>4</sub> ] 26	<i>P</i> <sub>2</sub> / <i>n</i>	-3.16	OC-6 (0.33)	JCSAPR-9 (1.81) CSAPR-9 (1.26)	 tegH <sub>2</sub>		[23]
[Fe <sup>III</sup> <sub>2</sub> Ho <sup>III</sup> (MeO) <sub>2</sub> (teg) <sub>2</sub> (NO <sub>3</sub> ) <sub>2</sub> (piv) <sub>4</sub> ] 28	<i>P</i> <sub>2</sub> / <i>n</i>	-3.19	OC-6 (0.35)	JCSAPR-9 (1.69) CSAPR-9 (1.18) TCTPR-9 (2.29)	 tegH <sub>2</sub>		[23]
[Fe <sup>III</sup> <sub>2</sub> Dy <sup>III</sup> (OH) <sub>2</sub> (dda) <sub>2</sub> (Hpdf) <sub>2</sub> (NO <sub>3</sub> ) <sub>4</sub> (H <sub>2</sub> O) <sub>1.5</sub> (MeOH) <sub>0.5</sub> ] 6MeCN 32	<i>P</i> <sub>2</sub> / <i>n</i>	-4.47	OC-6 (2.66)	CSAPR-9 (1.41) TCTPR-9 (2.40) MFF-9 (1.67)	 ddaH <sub>2</sub>  pdfH <sub>2</sub>	NO <sub>3</sub> <sup>-</sup> and H <sub>2</sub> O	[25]

the reported compounds have their cluster cores centred on a crystallographic inversion centre, the polyhedra only need to be assessed for one 3 d and one 4 f centre.

### 3. Survey of the {Fe<sup>III</sup><sub>2</sub>Ln<sub>2</sub>} Butterfly

#### 3.1. The first {Fe<sup>III</sup><sub>2</sub>Ln<sub>2</sub>} butterfly

Christou and co-workers<sup>[17]</sup> reported the first Fe<sup>III</sup>-4f butterfly to show SMM behaviour in 2006, namely [Fe<sup>III</sup><sub>2</sub>Ho<sub>2</sub>(m<sub>3</sub>-OH)<sub>2</sub>(teaH)<sub>2</sub>(O<sub>2</sub>CPh)<sub>4</sub>(NO<sub>3</sub>)<sub>2</sub>]·6MeCN (1) and [Fe<sup>III</sup><sub>2</sub>Ln<sub>2</sub>(m<sub>3</sub>-OH)<sub>2</sub>(teaH)<sub>2</sub>(O<sub>2</sub>CPh)<sub>4</sub>]·4MeCN·3H<sub>2</sub>O (Ln<sup>III</sup>=Tb<sup>III</sup> (2) or Dy<sup>III</sup> (3) and HO<sub>2</sub>CPh is benzoic acid) (see Table 1). These three compounds were prepared from a reaction of [Fe<sup>III</sup><sub>3</sub>O(O<sub>2</sub>CPh)<sub>6</sub>(H<sub>2</sub>O)<sub>3</sub>](O<sub>2</sub>CPh), Ln<sup>III</sup>(NO<sub>3</sub>)<sub>3</sub>·nH<sub>2</sub>O and teaH<sub>3</sub> in a ratio of 0.75:0.25:2 in MeCN at room temperature.

As explained above, the overall core structures can be described in terms of a Type I butterfly with the two Fe<sup>III</sup> ions occupying the body positions and the Ln<sup>III</sup> ions occupying the wing-tip positions (Figure 3). The core is stabilised by two μ<sub>3</sub>-OH<sup>-</sup> ligands, both bridging to two Fe<sup>III</sup> ions and one Ln<sup>III</sup> ion. Around the periphery of the cluster, two doubly deprotonated alcohol arms of the two teaH<sup>2-</sup> ligands, both displaying the μ<sub>3</sub>-η<sup>2</sup>:η<sup>2</sup>:η<sup>1</sup>:η<sup>1</sup> chelating and bridging coordination mode provide the four μ<sub>2</sub>-O bridges. Note that since the triethanolamine ligands contribute to the basic core {M<sub>4</sub>(μ<sub>3</sub>-O)<sub>2</sub>(μ<sub>2</sub>-O)<sub>4</sub>} structure we described above, we designate these as “main ligands”. The third, protonated arm of each triethanolamine ligand simply chelates to its respective outer Ln<sup>III</sup> ion. The molecular structure is completed by four bridging benzoate ligands which link the

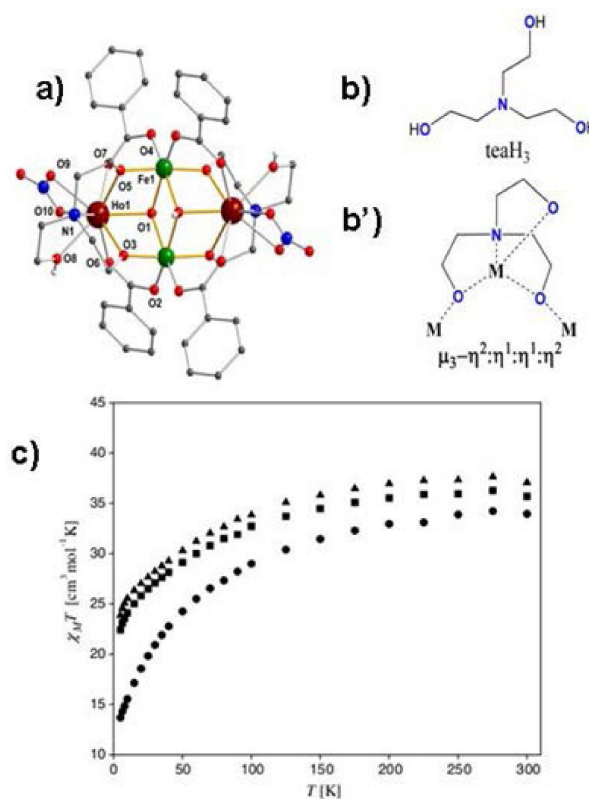


**Figure 3.** The structure for [Fe<sup>III</sup><sub>2</sub>Ho<sub>2</sub>(μ<sub>3</sub>-OH)<sub>2</sub>(teaH)<sub>2</sub>(O<sub>2</sub>CPh)<sub>4</sub>(NO<sub>3</sub>)<sub>2</sub>]·6MeCN (a); the coordination teaH<sub>3</sub> ligands (b) and the coordination mode of teaH<sub>3</sub> (b'); Plot of  $\chi T$  vs.  $T$  for complexes 1 {Fe<sup>III</sup><sub>2</sub>Ho<sub>2</sub>} (circle), 2 {Fe<sup>III</sup><sub>2</sub>Tb<sub>2</sub>} (square) and 3 {Fe<sup>III</sup><sub>2</sub>Dy<sub>2</sub>} (triangle). Adapted with permission from Ref. [17]. Copyright 2006, Elsevier.

central Fe<sup>III</sup> ions to the wing-tip Ln<sup>III</sup> ions and two chelating nitrates for compound 1 or else two further benzoate ligands for 2 and 3 which complete the coordination spheres of the lanthanide ions. These bridging and chelating ligands are designated as “co-ligands” by us and they generally derive from the metal starting salts and complexes.

The two Fe<sup>III</sup> ions are six coordinate with octahedral (OC-6) geometries and the two Ln<sup>III</sup> ions are nine coordinate with capped square antiprismatic (CSAPR-9) geometries (Table 1).

As explained above, the overall core structures can be described in terms of a Type I butterfly with the two Fe<sup>III</sup> ions occupying the body positions and the Ln<sup>III</sup> ions occupying the wing-tip positions (Figure 3). The core is stabilised by two μ<sub>3</sub>-OH<sup>-</sup> ligands, both bridging to two Fe<sup>III</sup> ions and one Ln<sup>III</sup> ion. Around the periphery of the cluster, two doubly deprotonated alcohol arms of the two teaH<sup>2-</sup> ligands, both displaying the μ<sub>3</sub>-η<sup>2</sup>:η<sup>2</sup>:η<sup>1</sup>:η<sup>1</sup> chelating and bridging coordination mode provide the four μ<sub>2</sub>-O bridges. Note that since the triethanolamine ligands contribute to the basic core {M<sub>4</sub>(μ<sub>3</sub>-O)<sub>2</sub>(μ<sub>2</sub>-O)<sub>4</sub>} structure we described above, we designate these as “main ligands”. The third, protonated arm of each triethanolamine ligand simply chelates to its respective outer Ln<sup>III</sup> ion.

The molecular structure is completed by four bridging benzoate ligands which link the central Fe<sup>III</sup> ions to the wing-tip Ln<sup>III</sup> ions and two chelating nitrates for compound 1 or else two further benzoate ligands for 2 and 3 which complete the coordination spheres of the lanthanide ions. These bridging and chelating ligands are designated as “co-ligands” by us and they generally derive from the metal starting salts and complexes. The two Fe<sup>III</sup> ions are six coordinate with octahedral (OC-6) geometries and the two Ln<sup>III</sup> ions are nine coordinate with capped square antiprismatic (CSAPR-9) geometries (Table 1).

Magnetic measurements revealed dominant antiferromagnetic interactions for all three compounds (Figure 3). The dynamic properties were investigated using ac susceptibility measurements and these indicate that both {Fe<sup>III</sup><sub>2</sub>Ho<sup>III</sup><sub>2</sub>} (1) and {Fe<sup>III</sup><sub>2</sub>Dy<sup>III</sup><sub>2</sub>} (3) show slow magnetic relaxation but without maximum above 1.8 K. Further micro-SQUID measurements on (1) and (3), though, revealed these compounds are SMMs showing hysteresis loops at lower temperatures. For {Fe<sup>III</sup><sub>2</sub>Ho<sup>III</sup><sub>2</sub>} the loops opening below 0.3 K were smooth (Figure 4, top) and assigned to the presence of intermolecular stacking interactions. The step-structured loops for {Fe<sup>III</sup><sub>2</sub>Dy<sup>III</sup><sub>2</sub>} opening below 1.1 K (Figure 4, bottom) were taken as indicative of a quantum tunnelling process (QTM). The fact that this relaxation occurs at zero-field precluded the possibility to extract a *U<sub>eff</sub>* value.

### 3.2. Systematic studies on Type I {Fe<sup>III</sup><sub>2</sub>Ln<sub>2</sub>} butterflies

#### 3.2.1. The ‘test bed’ series

The {Fe<sup>III</sup><sub>2</sub>Dy<sup>III</sup>} coordination cluster with the same essential core structure as that of the compound [Fe<sup>III</sup><sub>2</sub>Dy<sup>III</sup><sub>2</sub>(μ<sub>3</sub>-OH)<sub>2</sub>(teaH)<sub>2</sub>(O<sub>2</sub>CPh)<sub>6</sub>]·4MeCN·3H<sub>2</sub>O (3) discussed above crystal-

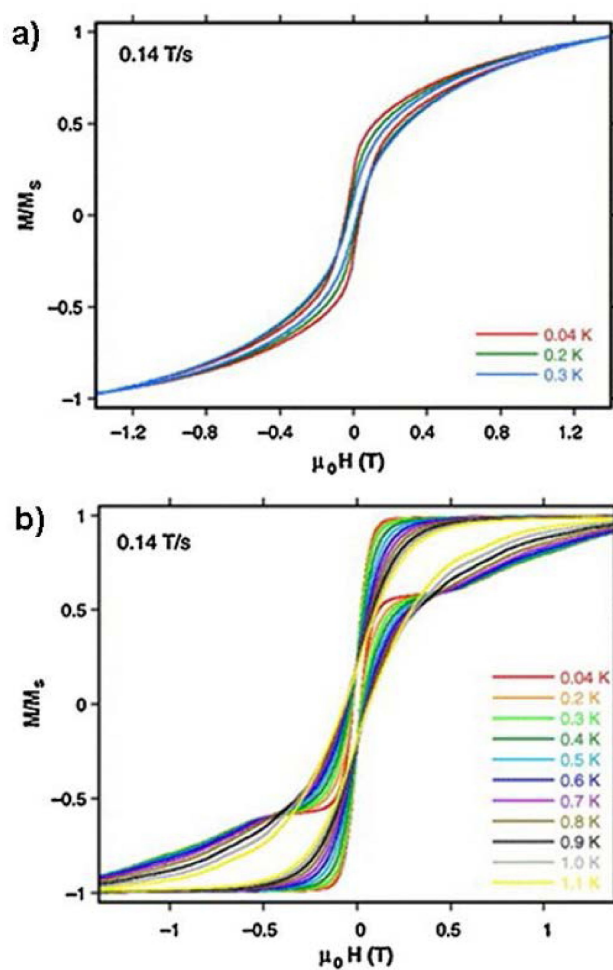


**Figure 4.** a) Hysteresis loop for [Fe<sup>III</sup><sub>2</sub>Ho<sup>III</sup><sub>2</sub>(μ<sub>3</sub>-OH)<sub>2</sub>(teaH)<sub>2</sub>(O<sub>2</sub>CPh)<sub>6</sub>(NO<sub>3</sub>)<sub>2</sub>]·6MeCN (1) measured on single crystals at 0.04, 0.2 and 0.3 K for a sweep rate of 0.14 T s<sup>-1</sup>. b) The same for [Fe<sup>III</sup><sub>2</sub>Dy<sup>III</sup><sub>2</sub>(μ<sub>3</sub>-OH)<sub>2</sub>(teaH)<sub>2</sub>(O<sub>2</sub>CPh)<sub>6</sub>]·4MeCN·3H<sub>2</sub>O (3) between 0.04 and 1.1 K. Adapted with permission from Ref. [17] Copyright 2006, Elsevier.

lises as [Fe<sup>III</sup><sub>2</sub>Dy<sup>III</sup><sub>2</sub>(μ<sub>3</sub>-OH)<sub>2</sub>(teaH)<sub>2</sub>(O<sub>2</sub>CPh)<sub>6</sub>]·6MeCN under our synthetic conditions.<sup>[18b]</sup>

This generic compound was selected for use as a “test-bed” for the following reasons (Figure 5):

- The complexes are structurally simple usually with one crystallographically independent Fe<sup>III</sup> and one crystallographically independent lanthanide site. This simplifies theoretical treatment and analysis.
- Choosing Fe as the 3d ion allows <sup>57</sup>Fe Mössbauer spectroscopy to be used as an additional technique which can give information about oxidation levels and spin states, local moments at the iron nuclei and spin-relaxation and, more importantly, about the anisotropy not only of the studied isotope, but also of elements interacting with this isotope.<sup>[26]</sup>
- Isostructural analogues with the same Fe<sup>III</sup> ions with all the available (i.e., not Pm) 4f ions can be synthesised. This allows for a systematic survey of the influence of the 4f ion on the electronic structure.

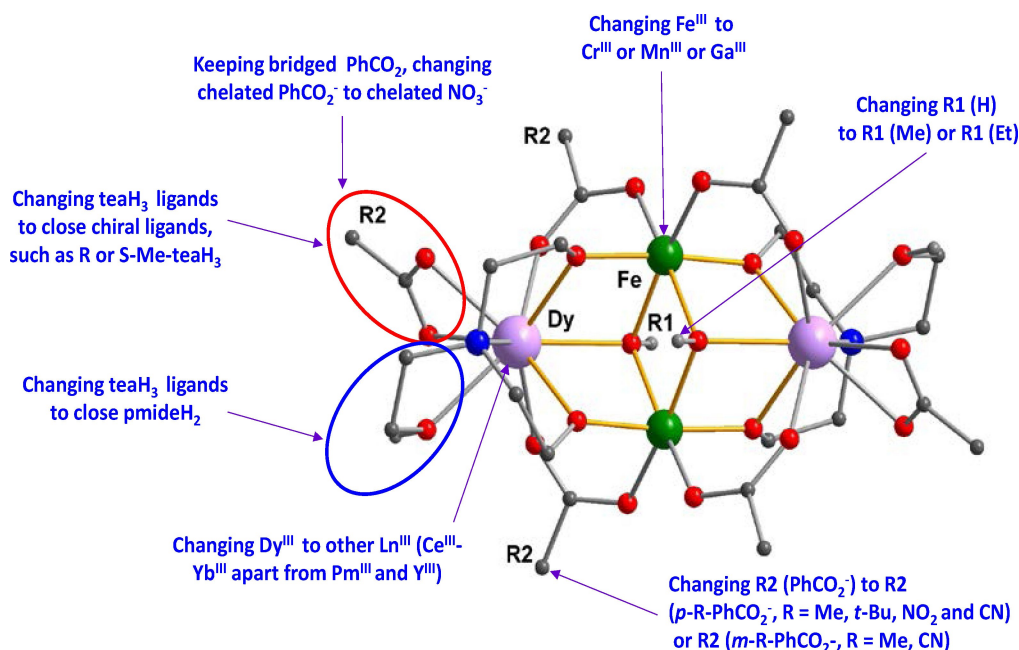
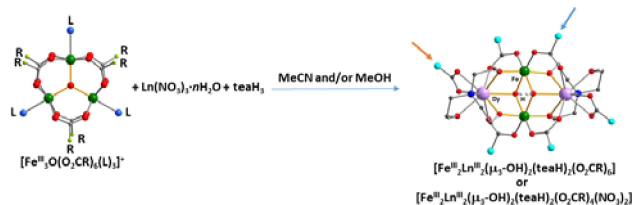


Figure 5. The tuning possibilities for the “test-bed”  $[\text{Fe}^{\text{III}}_2\text{Dy}^{\text{III}}(\mu_3\text{-OH})_2(\text{teaH})_2(\text{O}_2\text{CPh})_6] \cdot 6\text{MeCN}$  butterfly molecule.

- (iv) This cluster type is obtained (Scheme 2) by reacting triangular oxo-bridged trinuclear iron carboxylate complexes of general formula  $[\text{Fe}^{\text{III}}_3\text{O}(\text{O}_2\text{CR})_6(\text{L})_3](\text{X})$ , with  $\text{X} =$  anion and  $\text{L} = \text{H}_2\text{O}$ , py, solvent such as methanol or ethanol and/or carboxylic acid with the ligand triethanolamine ( $\text{H}_3\text{tea}$ ) and lanthanide salts.<sup>[27]</sup> Thus, it is possible to synthesise the  $[\text{Fe}^{\text{III}}_2\text{Ln}^{\text{III}}(\mu_3\text{-OH})_2(\text{teaH})_2(\text{O}_2\text{CR})_6]$  analogues starting from the appropriate iron trinuclear starting materials which can contain different *para*-substituted or *meta*-substituted benzoates as well as with other carboxylates and nitrate anions as the co-ligands.
- (v) The organic main ligand can be readily functionalised, facilitating a systematic investigation of the effect of organic substituents on the ligands on the magnetic properties of the complexes.



Scheme 2. The synthetic route to access  $\{\text{Fe}^{\text{III}}_2\text{Ln}^{\text{III}}\}$  butterflies. The starting material  $[\text{Fe}^{\text{III}}_3\text{O}(\text{O}_2\text{CR})_6(\text{L})_3]^+$  can be varied with differently substituted carboxylates and different terminal neutral ligands, L. In the product the substituent on the carboxylate is shown in turquoise. The blue arrow indicates that the bridging carboxylates always carry the substituent of the starting triangle. The orange arrow indicates that the chelating group on the Ln wingtips may also be this carboxylate or can be chelating nitrates introduced from the counterions of the starting materials.

A schematic representation of the synthetic pathways for the complexes in this review is given in Scheme 3.

### 3.2.2. Lanthanide ion effect

In order to investigate lanthanide ions effect of the magnetic anisotropy in the above  $\{\text{Fe}^{\text{III}}_2\text{Ln}^{\text{III}}\}$  system, a series of 13 isostructural analogues  $[\text{Fe}^{\text{III}}_2\text{Ln}^{\text{III}}(\mu_3\text{-OH})_2(\text{teaH})_2(\text{O}_2\text{CPh})_6]$  ( $\text{Ln} = \text{Ce}$  (4), Pr (5), Nd (6), Sm (7), Eu (8), Gd (9), Tb (2), Dy (3), Ho (10), Er (11), Tm (12), Yb (13), Y(14)) for all lanthanides from  $\text{Ce}^{\text{III}}$  to  $\text{Yb}^{\text{III}}$ , together with  $\text{Y}^{\text{III}}$  in high yields (Figure 6a), was prepared through modifying a previously published synthetic method.<sup>[18b]</sup> It was assumed that the compounds 2 and 3 are identical to

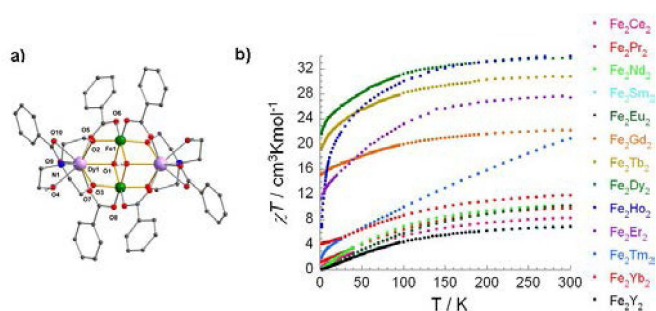
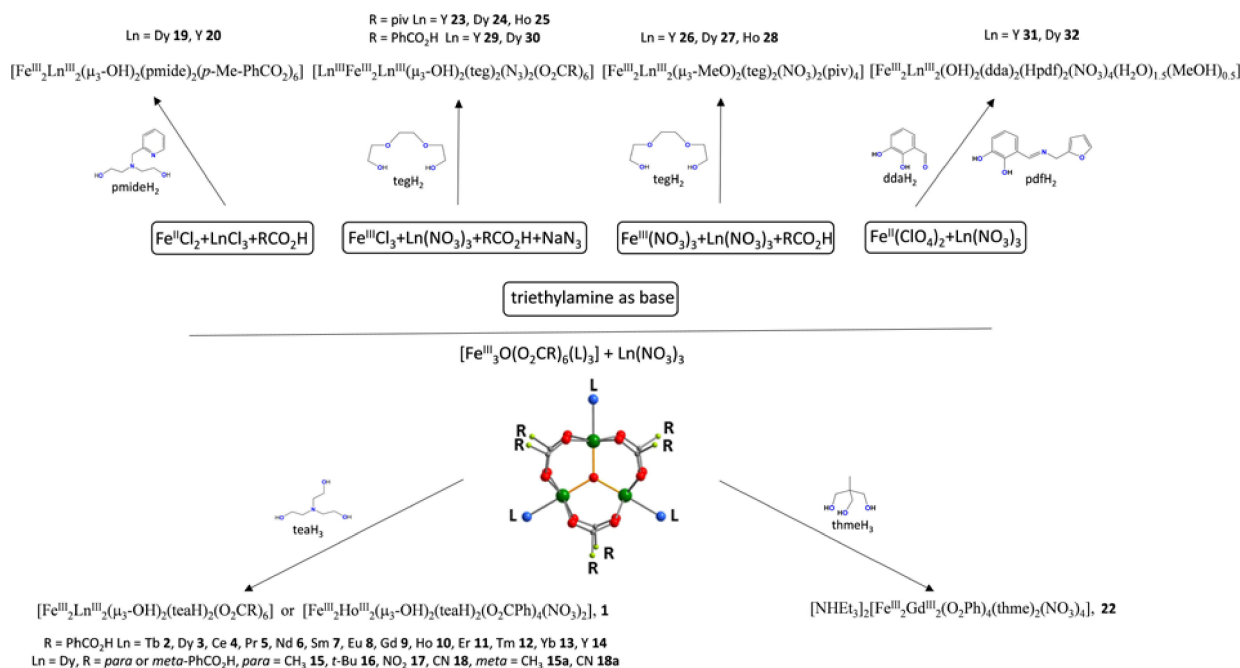


Figure 6. Molecular structures of  $[\text{Fe}^{\text{III}}_2\text{Ln}^{\text{III}}(\mu_3\text{-OH})_2(\text{teaH})_2(\text{O}_2\text{CPh})_6]$  ( $\text{Ln} = \text{Ce}$  (4), Pr (5), Nd (6), Sm (7), Eu (8), Gd (9), Tb (2), Dy (3), Ho (10), Er (11), Tm (12), Yb (13), Y(14)) (a); organic H-atoms and lattice solvent molecules omitted for clarity. Temperature-dependence of the  $\chi T$  product under 1000 Oe dc field for compounds 2–14 (b). Reprinted with permission from Ref. [18b] Copyright 2013, The Royal Society of Chemistry.





**Scheme 3.** Schematic representation of the synthetic relationships between the tetranuclear cluster system, showing the influence of Fe starting material, Ln salt, or ligand on the synthetic outcomes.

reported  $\{\text{Fe}^{\text{III}}_2\text{Tb}^{\text{III}}_2\}$  and  $\{\text{Fe}^{\text{III}}_2\text{Dy}^{\text{III}}_2\}$  butterflies<sup>[17]</sup> discussed above.

Dc susceptibilities measurements on the compounds revealed overall antiferromagnetic coupling (Figure 6b) between magnetic centres. An exchange constant of  $J_{\text{Fe-Fe}} = -6.53(5) \text{ cm}^{-1}$  and a g value of 2.0 were found from the best fit of the  $\chi T$  versus T curve of  $\{\text{Fe}^{\text{III}}_2\text{Y}_2\}$  (**14**) using the Spin Hamiltonian  $H = -2JS_1S_2$ . The isotropic spin model also has been used successfully to fit the data for  $\{\text{Fe}^{\text{III}}_2\text{Gd}_2\}$  (**9**) where it was found that the antiferromagnetic interaction between Fe<sup>III</sup> ions also dominates here with  $J_{\text{Fe-Fe}} = -6.71(4) \text{ cm}^{-1}$ , in good agreement with the value found for  $\{\text{Fe}^{\text{III}}_2\text{Y}_2\}$ . Furthermore, weak ferromagnetic interactions between Fe<sup>III</sup> and Gd<sup>III</sup> ions with  $J_{\text{Fe-Gd}} = +0.18(1) \text{ cm}^{-1}$  were found. Ac susceptibility measurements revealed that only  $\{\text{Fe}^{\text{III}}_2\text{Dy}^{\text{III}}_2\}$  shows slow magnetic relaxation (Figure 7) with an energy barrier  $U_{\text{eff}} = 16.21 \text{ K}$  and

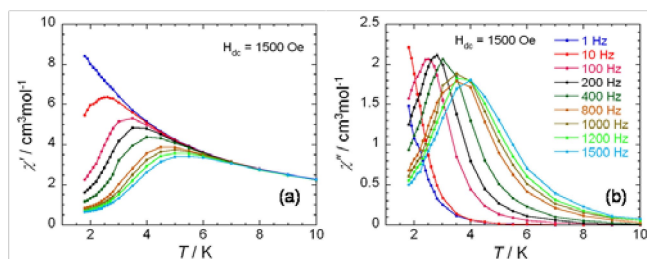


**Figure 7.** Temperature dependence of the in-phase (left) and out-of-phase (right) components of the ac magnetic susceptibility, for  $\{\text{Fe}^{\text{III}}_2\text{Dy}^{\text{III}}_2\}$  (**3**) under 1500 Oe applied dc field. Reprinted with permission from Ref. [18b] Copyright 2013, The Royal Society of Chemistry.

relaxation time  $\tau_0 = 1.9 \times 10^{-6} \text{ s}$  under a 1000 Oe dc field with no ac signals observable for the other twelve compounds even under applied dc field.

Mössbauer spectra on the compounds containing Y, Gd, Ho, Dy and Tb only showed the onset of a magnetic spectrum for the Dy analogue when measured at 3 K (Figure 8). Although the highly anisotropic Tb<sup>III</sup> containing compound might also be expected to show a magnetic spectrum, the observed difference in behaviour seen between  $\{\text{Fe}^{\text{III}}_2\text{Dy}_2\}$  and  $\{\text{Fe}^{\text{III}}_2\text{Tb}_2\}$  is likely to be a consequence of the Kramers and non-Kramers nature of these two ions, respectively leading to a larger effect of the non-axial ligand-field potential on the Tb complex. EPR (Electron Paramagnetic Resonance spectroscopy) study and theoretical ab initio calculations investigation also suggest that the peculiar anisotropy of Dy<sup>III</sup> ions is responsible for the presence of slow magnetic relaxation, which was experimentally confirmed by several complementary methods. relationship with different substituents in order to enhance the blocking temperature of SMMs.

The use of complementary techniques allows comparisons between a series of isostructural butterfly compounds with varying lanthanide ions and electronic configurations and anisotropies to be made. This series of  $\{\text{Fe}^{\text{III}}_2\text{Ln}_2\}$  butterfly compounds is also suited to be a test-bed for the next stage of study on co-ligand substituent effect which is described for a series of compounds containing the Dy<sup>III</sup> ion in the next section. This also leads to the ultimate aim of learning how to exploit the individual nature of each lanthanide.

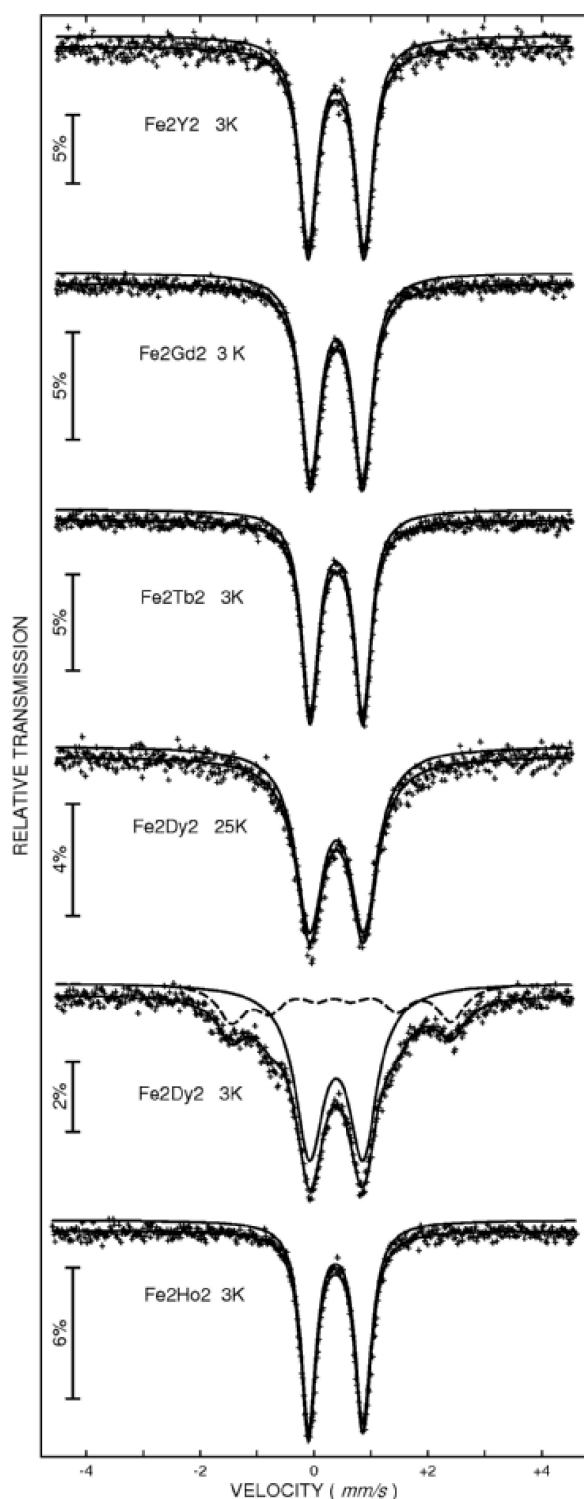


**Figure 8.** The  $^{57}\text{Fe}$  Mössbauer spectra for  $[\text{Fe}^{\text{III}}_2\text{Y}_2]$  (14),  $[\text{Fe}^{\text{III}}_2\text{Gd}_2]$  (9),  $[\text{Fe}^{\text{III}}_2\text{Tb}_2]$  (2), and  $[\text{Fe}^{\text{III}}_2\text{Ho}_2]$  (10) at 3 K as well as  $[\text{Fe}^{\text{III}}_2\text{Dy}_2]$  (3) at 3 K and 25 K. Reprinted with permission from Ref. [18b]. Copyright 2013, The Royal Society of Chemistry.

### 3.2.3. Co-ligand effect

In order to investigate how the co-ligand substituent influences magnetic properties, a family of  $[\text{Fe}^{\text{III}}_2\text{Dy}_2(\mu_3\text{-OH})_2(\text{teaH})_2(p\text{-R-PhCO}_2)_6]$ , where  $\text{R}=\text{H}$  (3), Me (15),  $t\text{-Bu}$  (16),  $\text{NO}_2$  (17), or CN (18),<sup>[18a]</sup> compounds with different *para*-substituted benzoate ligands were synthesised. This variation of  $\text{R}$  does not change the overall molecular structure (Figure 9a), which is analogous to  $[\text{Fe}^{\text{III}}_2\text{Dy}_2(\mu_3\text{-OH})_2(\text{teaH})_2(p\text{-H-PhCO}_2)_6]$  (3) and can be prepared in a similar way, using slight variations in reaction conditions.

According to analysis for the  $[\text{Fe}^{\text{III}}_2\text{Y}^{\text{III}}_2(\mu_3\text{-OH})_2(\text{teaH})_2(p\text{-H-PhCO}_2)_6]$  analogue, the central  $[\text{Fe}^{\text{III}}_2]$  unit is antiferromagnetically coupled and has an  $S=0$  ground state. This allows the results of the subtle changes in the orientation of the  $\text{Dy}^{\text{III}}$ 's principal magnetic anisotropy axes on changing the substituent on the benzoate to be probed (shown in Figure 9b, for each substituent). Using  $^{57}\text{Fe}$  Mössbauer spectroscopy a significant change in the internal field at the  $^{57}\text{Fe}$  ion was detected. This was attributed to the differing environment of the  $\text{Dy}^{\text{III}}$  ions polarising the  $^{57}\text{Fe}$  "electron cloud" in subtly different ways (Figure 10). The results clearly indicate the significant influence a seeming remote ligand substituent can have on the electronic structure and magnetic properties of these  $\{\text{Fe}^{\text{III}}_2\text{Dy}^{\text{III}}_2\}$  compounds.

Given that with this family of  $\{\text{Fe}^{\text{III}}_2\text{Dy}_2\}$  coordination clusters with different *para*-substituted benzoate ligands we could show that the influence of the *para*-substituent  $\text{R}$  on the benzoate can be gauged using  $^{57}\text{Fe}$  Mössbauer spectroscopy and, indeed, related to Hammett constants of the individual benzoic acids, it was obviously of interest to study the effect on the electronic structure and anisotropy of the core on moving a substituent from the *para* to the *meta* position on the benzoate. This is synthetically not so straightforward, but it proved possible to crystallise and compare the properties of two selected pairs of *para/meta* congeners:  $[\text{Fe}^{\text{III}}_2\text{Dy}_2(\mu_3\text{-OH})_2(\text{teaH})_2(p\text{-R-PhCO}_2)_6]$  ( $\text{R}=\text{CN}$  (18) and Me (15)) and  $[\text{Fe}^{\text{III}}_2\text{Dy}_2(\mu_3\text{-OH})_2(\text{teaH})_2(m\text{-R-PhCO}_2)_6]$  ( $\text{R}=\text{CN}$  (18a) and Me (15a)) (Figure 11), labelled as *p*-CN, *p*-Me, *m*-CN and *m*-Me in the following discussion for these four compounds respectively. They are closely isostructural,

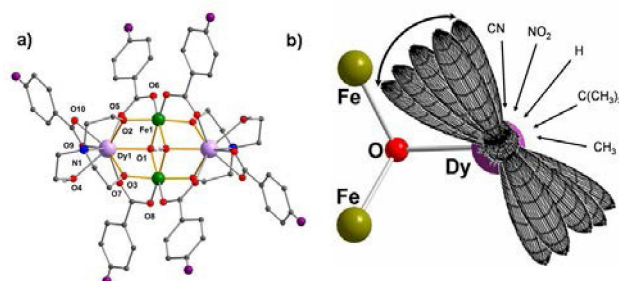


**Figure 9.** Molecular structure of  $[\text{Fe}^{\text{III}}_2\text{Dy}_2(\mu_3\text{-OH})_2(\text{teaH})_2(\text{para-R-PhCO}_2)_6]$  (organic H atoms have been omitted for clarity). a. The purple substituents at the *para* positions of the benzoic rings are H (3), Me (15),  $t\text{-Bu}$  (16),  $\text{NO}_2$  (17), or CN (18); right, Schematic arrangements of the local magnetic moments (anisotropic axes) of a  $\text{Dy}^{\text{III}}$  ion relative to the  $[\text{Fe}^{\text{III}}_2]$  unit. b. Reprinted with permission from Ref. [18a] Copyright 2011, American Chemical Society.

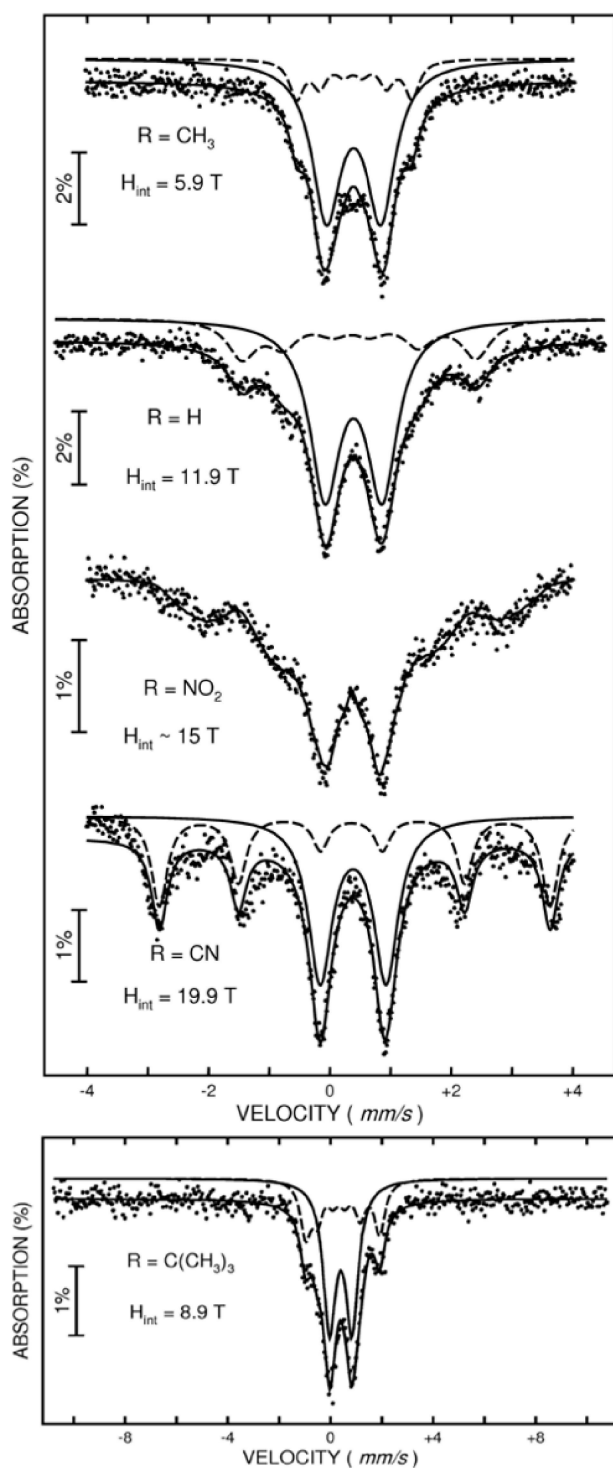


**Figure 10.** The  $^{57}\text{Fe}$  Mössbauer spectra of H (3), Me (15),  $^t\text{Bu}$  (16),  $\text{NO}_2$  (17), or CN (18) in zero applied field at 3.0 K. On left-hand side of each spectrum, the value of the internal hyperfine field  $H_{\text{int}}$  determined from the sextet is given. For compound 16, the distribution of probability for the magnetic hyperfine field was used. Reprinted with permission from Ref. [18a]. Copyright 2011, American Chemical Society.

differing only in the *para*- or *meta*-substituent on their benzoate rings.

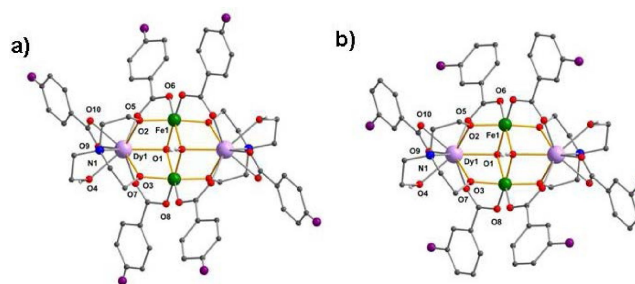


**Figure 11.** The structures of  $[\text{Fe}^{\text{III}}_2\text{Dy}_2(\mu_3\text{-OH})_2(\text{teaH})_2(p\text{-R-PhCO}_2)_6]$ , purple is  $R = p\text{-CN}$  (18) or  $p\text{-Me}$  (15), a and  $[\text{Fe}^{\text{III}}_2\text{Dy}_2(\mu_3\text{-OH})_2(\text{teaH})_2(m\text{-R-PhCO}_2)_6]$ ,  $R = m\text{-CN}$  (18a) or  $m\text{-Me}$  (15a), b. Reprinted with permission from Ref. [19] Copyright 2013, The Royal Society of Chemistry.

The dc susceptibilities indicated that all compounds show overall antiferromagnetic coupling between the magnetic centres (Figure 12) as observed for the previously described  $\{\text{Fe}^{\text{III}}_2\text{Ln}_2\}$  systems.

The ac susceptibility measurements showed that the SMM behaviour for the four compounds follows the trend,  $p\text{-Me} < m\text{-Me} < m\text{-CN} < p\text{-CN}$  under zero field. Whereas  $m\text{-Me}$  shows only a very weak ac signal,  $p\text{-Me}$  shows no ac signal. For the  $p\text{-CN}$  complex the blocking temperature for the relaxation of magnetisation is ca. 3 K at 1500 Hz whereas for the  $m\text{-CN}$  complex, no maximum was observed in the ac signals (Figure 13a). These observations indicate that there are indeed clear effects on the magnetic properties resulting from not only varying the nature of substituent from electron-withdrawing  $-\text{CN}$  and electron-donating  $-\text{Me}$ , but also the position of these on the ring, that is, *para* versus *meta*.

From these results it was concluded that at low temperatures there are different anisotropic properties of the dyspro-

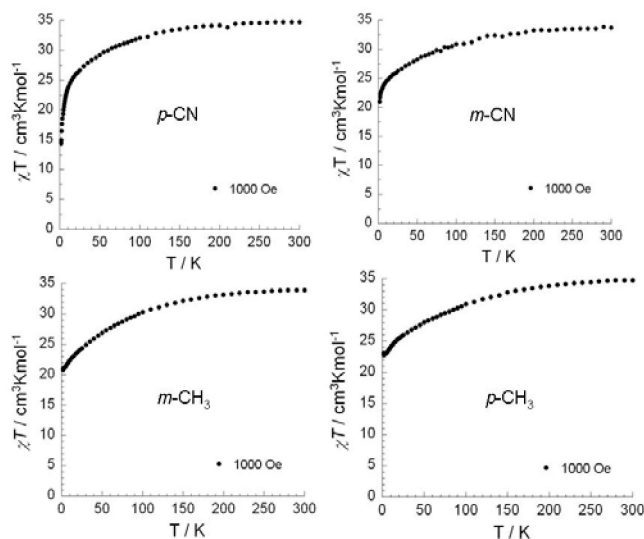


**Figure 12.**  $\chi T$  versus  $T$  plots at 1000 Oe for  $p\text{-CN}$  (18),  $m\text{-CN}$  (18a),  $p\text{-Me}$  (15) and  $m\text{-Me}$  (15a). Reprinted with permission from Ref. [19] Copyright 2013, The Royal Society of Chemistry.



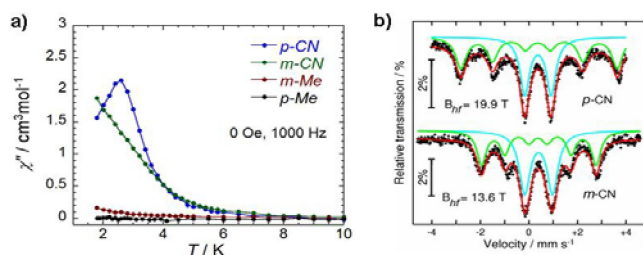


**Figure 13.** Temperature dependence of the out-of-phase components of the ac magnetic susceptibility at 1000 Hz for compounds under zero dc field (left) and Mössbauer spectra of polycrystalline  $[\text{Fe}^{\text{III}}_2\text{Dy}^{\text{III}}_2(\mu_3\text{-OH})_2(\text{teaH})_2(\text{R-PhCO}_2)_6]$ , where  $\text{R} = p\text{-CN}$  and  $m\text{-CN}$ , at 3 K in zero applied magnetic field (right). On left-hand side of each spectrum, the value of the internal hyperfine field  $B_{\text{hf}}$  determined from the sextet is given. Reprinted with permission from Ref. [19] Copyright 2013, The Royal Society of Chemistry.

sium moments, which in turn should result in either stronger or weaker magnetic interactions with the iron nuclei. The results of  $^{57}\text{Fe}$  Mössbauer spectroscopy on polycrystalline samples both with and without applied fields indicated that along the series the magnetic hyperfine field  $B_{\text{hf}}$  at 3 K decreases from 19.9 to 5.9 T in the order  $p\text{-CN}$ ,  $m\text{-CN}$ ,  $m\text{-Me}$ ,  $p\text{-Me}$  (i.e., in the order **18**, **18a**, **15a**, **15**) (Figure 13b). Overall, the results of these investigations revealed how subtle changes in the nature and position of the substituents on a benzoate ligand can fine-tune the direction of the orientation of the principal anisotropy axis of the crystal field and exert a significant impact on the magnetic behaviour of the  $\text{Dy}^{\text{III}}$  ion even though the co-ligand substituents are remote from metal centres. Clearly, the anisotropy of  $\text{Dy}^{\text{III}}$  is very responsive to minor perturbations in the ligand environment as well as extremely sensitive to the strength of the chemical bond.

Furthermore, in order to gain insights into the effects of subtle changes to the co-ligands in the test bed, the series of  $[\text{Fe}^{\text{III}}_2\text{Dy}^{\text{III}}_2(\text{OH})_2(\text{teaH})_2(\text{RC}_6\text{H}_4\text{COO})_6]$  compounds,  $\text{R} = m\text{-CN}$  **18a**,  $p\text{-CN}$  **18**,  $m\text{-Me}$  **15a**,  $p\text{-NO}_2$  **17**, and  $p\text{-Me}$  **15**, were further analysed using ab initio calculations and EPR measurements.<sup>[28]</sup> The results indicate the interaction parameters for the  $\text{Fe}^{\text{III}}\text{-Fe}^{\text{III}}$  pair increase with the  $\text{Fe}^{\text{III}}\text{-O-Fe}^{\text{III}}$  angle and  $\text{Fe-Fe}$  distance. On the contrary, the  $\text{Fe}^{\text{III}}\text{-Dy}^{\text{III}}$  interaction decreases when the  $\text{Dy}^{\text{III}}\text{-O-Fe}^{\text{III}}$  angle and  $\text{Dy}^{\text{III}}\text{-Fe}^{\text{III}}$  distance increase. The BS-DFT calculations and simulations of the magnetic susceptibility data revealed that the  $\text{Fe}^{\text{III}}\text{-Fe}^{\text{III}}$  interaction in all compounds is much stronger than the  $\text{Dy}^{\text{III}}\text{-Fe}^{\text{III}}$  and  $\text{Dy}^{\text{III}}\text{-Dy}^{\text{III}}$  interactions. It was found that the  $\text{Fe}^{\text{III}}\text{-Fe}^{\text{III}}$  interaction must be taken into account to describe the energy gap between the two lowest exchange doublets. The  $\text{Dy}^{\text{III}}\text{-Dy}^{\text{III}}$  dipolar and exchange interactions are very weak in all these compounds, which leads to a small separation of the lowest two exchange doublets and this is also supported by the EPR spectroscopy. This small gap enables the relaxation of magnetisation to proceed by a spin flip on individual dysprosium ions. Given that both doublets are almost completely populated in the investigated temperature range, it appears that the compounds demonstrate poor SMM behaviour. This is because at temperatures exceeding several times

the  $\text{Dy}^{\text{III}}\text{-Dy}^{\text{III}}$  exchange/dipolar splitting, the latter is no longer operative, so the blockage of magnetisation originates only at individual uncoupled dysprosium ions. However, the transversal components of the  $g$  tensors of the ground Kramers doublets of the dysprosium ions are relatively large, thus allowing unquenched quantum tunnelling of magnetisation, which impedes the occurrence of magnetisation blockage.

### 3.2.4. Main-ligand effect

#### 3.2.4.1. teaH<sup>-</sup> to pmide<sup>-</sup>

A further possibility for tuning the magnetic properties of these butterfly compounds is to change the main teaH<sub>3</sub> ligand to analogues of this molecule. This was explored for the compounds  $[\text{Fe}^{\text{III}}_2\text{Ln}_2(\mu_3\text{-OH})_2(\text{pmide})_2(p\text{-Me-PhCO}_2)_6]$  ( $\text{Ln} = \text{Dy}$ , **19** and  $\text{Y}$ , **20**) (see Figure 14a) as well as the analogue  $[\text{Al}^{\text{III}}_2\text{Dy}^{\text{III}}_2(\mu_3\text{-OH})_2(\text{pmide})_2(p\text{-Me-PhCO}_2)_6]$  (**21**), where  $\text{pmideH}_2 = N\text{-}(2\text{-pyridylmethyl})\text{-iminodiethanol}$  (see Figure 14b). The compounds are essentially isostructural to the  $[\text{Fe}^{\text{III}}_2\text{Dy}^{\text{III}}_2(\mu_3\text{-OH})_2(\text{teaH})_2(p\text{-Me-PhCO}_2)_6]$  (**15**) compound.<sup>[20,29]</sup>

As can be seen from the structure of the  $\text{Dy}^{\text{III}}$  compound **19** shown in Figure 14a, the protonated chelating alcohol arm of the teaH<sub>3</sub> ligand which is attached to the  $\text{Ln}^{\text{III}}$  centres has been replaced by a picolyl arm. The dc magnetic measurements revealed the expected dominant antiferromagnetic interactions between the magnetic centres for the  $\{\text{Fe}^{\text{III}}_2\text{Ln}_2\}$  systems as was the case for the previously reported  $\{\text{Fe}^{\text{III}}_2\text{Ln}_2\}$  systems. For  $\{\text{Al}^{\text{III}}_2\text{Dy}_2\}$  there are dominant ferromagnetic interactions between the two distant  $\text{Dy}^{\text{III}}$  ions. Through the analysis and comparison of  $\chi T$  versus  $T$  plots for the three compounds (Figure 15) it was concluded that there is a very weak  $\text{Fe}^{\text{III}}\text{-Dy}^{\text{III}}$  interaction. Ac susceptibility measurements indicated that there is a slow magnetic relaxation, but without any maxima for the measurement under zero field. Under an applied dc field of 1000 Oe temperature dependent in and out of phase signals with maxima were observed for  $\{\text{Fe}^{\text{III}}_2\text{Dy}^{\text{III}}_2\}$  (Figure 16). The energy barrier found by fitting to an Arrhenius equation,  $\tau = \tau_0 \exp(U_{\text{eff}}/kT)$ , gave  $U_{\text{eff}} = 16.2$  K ( $11.2$   $\text{cm}^{-1}$ ) with  $\tau_0 = 2.6 \times 10^{-6}$  s, which are similar parameters to those found for the analogue

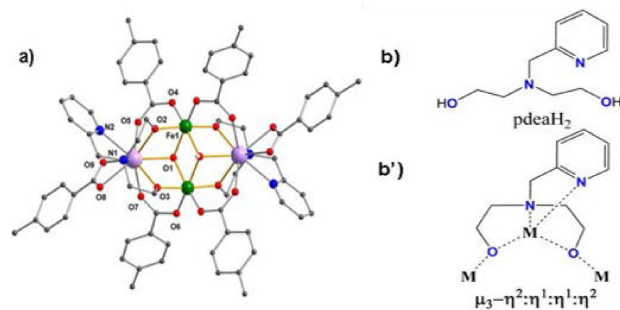


**Figure 14.** The structure of  $[\text{Fe}^{\text{III}}_2\text{Dy}^{\text{III}}_2(\mu_3\text{-OH})_2(\text{pdeaH}_2)_2(p\text{-Me-PhCO}_2)_6]$ , **19** (a); the coordination  $\text{pmideH}_2$  ligands (b) and the coordination mode of  $\text{pmideH}_2$  (b'). Reprinted with permission from Ref. [20] Copyright 2016, The Royal Society of Chemistry.

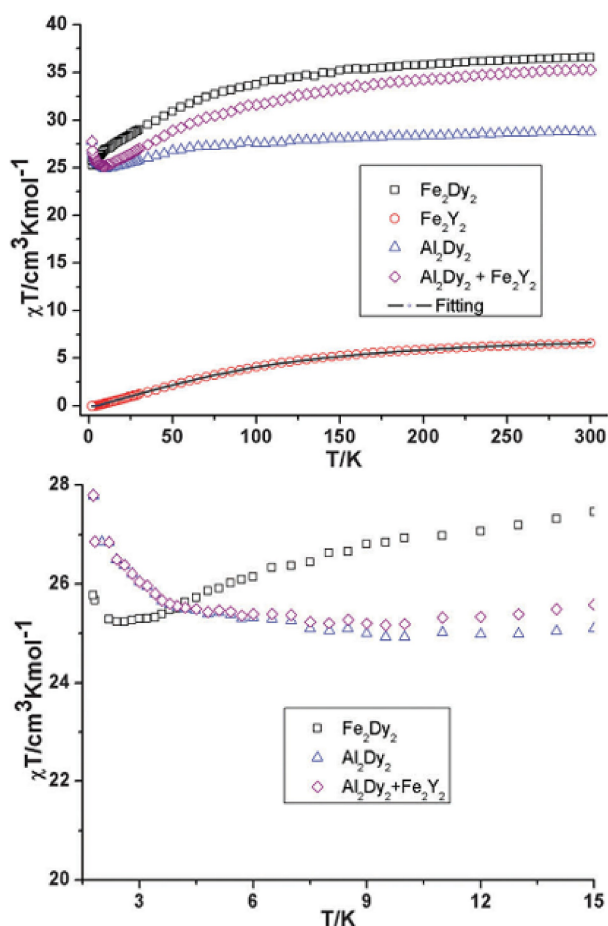


**Figure 15.** Temperature dependence (left) of the  $\chi T$  product at 300 Oe for **19**,  $\{\text{Fe}^{\text{III}}_2\text{Dy}_2\}$ , **20**,  $\{\text{Fe}^{\text{III}}_2\text{Y}_2\}$  (the solid line is the best fit to the experimental data for **20**) and **21**,  $\{\text{Al}^{\text{III}}_2\text{Dy}_2\}$ . The comparison curves (right) of  $\{\text{Fe}^{\text{III}}_2\text{Dy}_2\}$  and  $\{\text{Al}^{\text{III}}_2\text{Dy}_2\} + \{\text{Fe}^{\text{III}}_2\text{Y}_2\}$  along with the curve for **21**,  $\{\text{Al}^{\text{III}}_2\text{Dy}_2\}$  enlarged in the region below 15 K. Reprinted with permission from Ref. [20] Copyright (2016) The Royal Society of Chemistry.

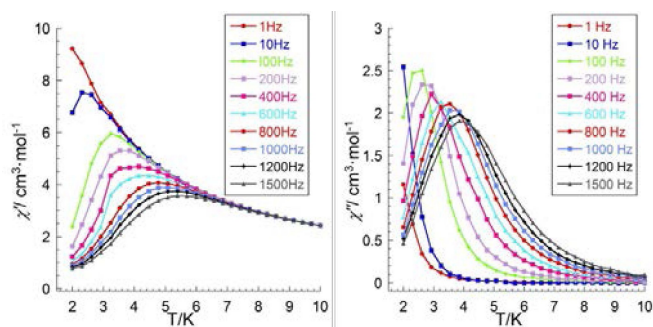


**Figure 16.** Temperature dependence of the in phase (left) and out-of-phase (right) components of the ac magnetic susceptibility at different frequencies for **19**  $\{\text{Fe}^{\text{III}}_2\text{Dy}_2\}$  at 1000 Oe. Reprinted with permission from Ref. [20] Copyright 2016, The Royal Society of Chemistry.

$[\text{Fe}^{\text{III}}_2\text{Dy}_2(\mu_3\text{-OH})_2(\text{tea})_2(p\text{-Me-PhCO}_2)_6]$  **15** containing the teaH<sub>3</sub> main ligand and *p*-Me-PhCO<sub>2</sub> co-ligand. There is no ac signal for  $\{\text{Fe}^{\text{III}}_2\text{Y}_2\}$  even under applied dc field, as would be expected, but typical SMM behaviour was observed for  $\{\text{Al}^{\text{III}}_2\text{Dy}_2\}$  under

zero field with an energy barrier  $U_{\text{eff}} = 38.7$  K and  $\tau_0 = 1.06 \times 10^{-6}$  s which must result from the presence of the Dy centres. The fact that the energy barrier is more than double that found for the  $\{\text{Fe}^{\text{III}}_2\text{Dy}_2\}$  compound is a common feature for 3d–4f coordination clusters. A general observation is that the relatively small but significant exchange coupling between 3d and 4f ions decreases the observed energy barrier with the respect to values found for the free, non-exchange coupled 4f ions. This decreases often compensated for by the fact that in the exchange coupled systems, quantum tunnelling of the magnetisation at zero-field is often suppressed. In the 4f single ion case it proves a significant challenge to avoid this zero-field tunnelling. This can also be described as a useful synthetic tool to force the system to go further up the energy barrier – what is lost in barrier height is compensated for through zero-field tunnelling suppression. This also has been observed in  $\{\text{Co}^{\text{II}}_2\text{Dy}^{\text{III}}_2\}$  butterfly complexes.<sup>[30]</sup>

For the  $\{\text{Fe}^{\text{III}}_2\text{Dy}_2\}$  compound ac susceptibility measurements in this case showed that there are at least three relaxation processes which could be revealed through the application of appropriate static fields. To explore this further, <sup>57</sup>Fe Mössbauer spectroscopy was used and well-resolved nuclear hyperfine structures could be observed. This demonstrated that on the Mössbauer timescale, without applied fields or else with small applied fields, the iron nuclei experience three or more super-hyperfine fields arising from the slow magnetisation reversal of the strongly polarised fields of the Dy<sup>III</sup> ions (Figure 17). This underlines the importance of using measurements running on different timescales in order to explore the relaxation processes in SMMs.

### 3.2.4.1.1. Lanthanide ion effect in $[\text{Fe}^{\text{III}}_2\text{Dy}_2(\mu_3\text{-OH})_2(\text{pimde})_2(p\text{-Me-PhCO}_2)_6]$

The selected isostructural analogues of  $[\text{M}^{\text{III}}_2\text{Er}_2(\mu_3\text{-OH})_2(\text{pimde})_2(p\text{-Me-PhCO}_2)_6]$  ( $M = \text{Fe}$  **19a** and Al **21a**) were also synthesised and their magnetic behaviour investigated.<sup>[21]</sup> Both compounds show field-induced single molecule magnet (SMM) behaviour. The results reinforce the widely held belief that Dy<sup>III</sup> containing 3d–4f compounds generally “perform” better as SMMs than those with other Kramers ions (in this case Er<sup>III</sup>). In-depth alternating current measurements under different dc fields on the  $\{\text{Fe}_2\text{Er}_2\}$  compound reveal that the Fe<sup>III</sup>–Fe<sup>III</sup> and Fe<sup>III</sup>–Er interactions speed up the relaxation and decrease the energy barrier height of the SMM in comparison with the  $\{\text{Al}_2\text{Er}_2\}$  case. The field induced SMM nature of  $\{\text{Fe}^{\text{III}}_2\text{Er}_2\}$  **19a** further revealed the sensitivity of the main ligand since no ac signal was observed for  $[\text{Fe}^{\text{III}}_2\text{Er}_2(\mu_3\text{-OH})_2(\text{teaH})_2(\text{O}_2\text{CPh})_6]$  **11**, even though the unsubstituted PhCOO<sup>−</sup> ligand gives better performance than *p*-Me-PhCOO<sup>−</sup> as known from the  $\{\text{Fe}^{\text{III}}_2\text{Ln}_2\}$  butterfly system.

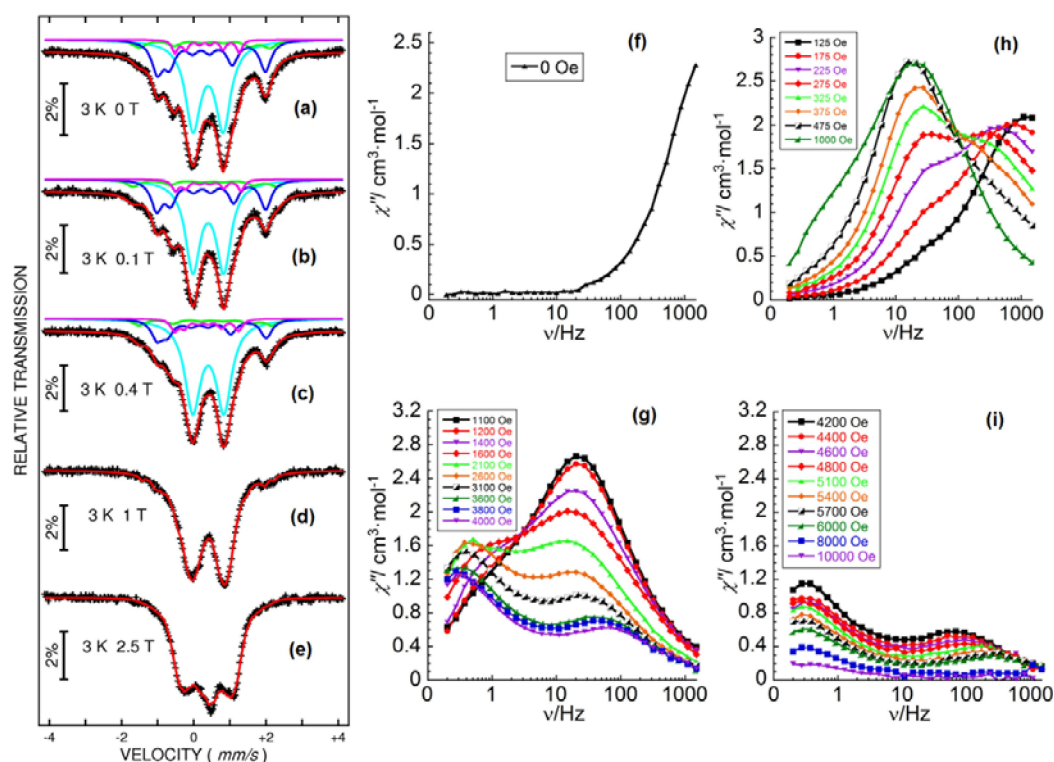


**Figure 17.** (a–e)  $^{57}\text{Fe}$  Mössbauer spectra of  $\{\text{Fe}^{\text{III}}_2\text{Dy}^{\text{III}}\}$  **19** at 3 K in zero- and applied external dc fields (0.1, 0.4, 1 and 2.5 T). (f–i) Frequency dependence of the out-of-phase ac susceptibility component for **19**  $\{\text{Fe}^{\text{III}}_2\text{Dy}^{\text{III}}\}$  at 2 K under different dc fields (0–10000 Oe corresponding to 0–1 T). The correspondence between the results from the Mössbauer measurements and the ac susceptibility data can be seen by comparing the spectrum in (a) with the trace in (f); in (b) with the 1000 Oe trace in (h); in (c) with the 4000 Oe trace in (g) and in (d) with the 10000 Oe trace in (i). Reprinted with permission from Ref. [20] Copyright 2016, The Royal Society of Chemistry.

### 3.2.4.1.2. Transition metal ion effect in $[\text{Fe}^{\text{III}}_2\text{Dy}^{\text{III}}(\mu_3\text{-OH})_2(\text{pimde})_2(\text{p-Me-PhCO}_2)_6]$

For the  $[\text{Fe}^{\text{III}}_2\text{Dy}^{\text{III}}(\mu_3\text{-OH})_2(\text{pimde})_2(\text{p-Me-PhCO}_2)_6]$  system, it was also possible to change the  $\text{Fe}^{\text{III}}$  ions to  $\text{Cr}^{\text{III}}$  and  $\text{Mn}^{\text{III}}$  ions, resulting in the isostructural  $[\text{M}^{\text{III}}_2\text{Dy}^{\text{III}}(\mu_3\text{-OH})_2(\text{pimde})_2(\text{p-Me-PhCO}_2)_6]$  ( $\text{M} = \text{Cr}$  or  $\text{Mn}$ ) as well as their Y analogues. This system provides a Type I core example where the central trivalent 3d ions can also be replaced by diamagnetic  $\text{Al}^{\text{III}}$ . The  $\text{Dy}^{\text{III}}$  ions are thus more isolated through the deletion of the paramagnetic  $\text{M}^{\text{III}}$  and the  $\text{Dy}^{\text{III}}$  single ion contribution can be seen. This allows for an ordering of influence of the nature of the trivalent 3d ion electron configuration in the  $\text{M}^{\text{III}} = \text{Cr}$ ,  $\text{Mn}$ ,  $\text{Fe}$  **37** analogues ( $[\text{M}^{\text{III}}_2\text{Dy}^{\text{III}}(\text{OH})_2(\text{pdea})_2(\text{p-Me-PhCO}_2)_6]$ ) to be assessed in terms of observed magnetic properties, backed up by ab initio and DFT calculations (Table 2). An ordering of the ions as  $d^4 > d^5 > d^3$  ( $\text{Mn}^{\text{III}}$ ,  $\text{Fe}^{\text{III}}$ ,  $\text{Cr}^{\text{III}}$ ) was established in terms of observation of maxima for the out-of-phase ac signals. The  $\text{Mn}^{\text{III}}$  h.s. ion also contributes anisotropy to the system as a result of the axial J–T distortion. The results suggest that altering the 3d<sup>III</sup> ions can affect the single-ion properties and the nature and the magnitude of the 3d<sup>III</sup>–3d<sup>III</sup>, 3d<sup>III</sup>– $\text{Dy}^{\text{III}}$  as well as the  $\text{Dy}^{\text{III}}$ – $\text{Dy}^{\text{III}}$  magnetic interactions to improve the SMM properties within this motif by significantly suppressing or quenching the quantum tunnelling of magnetisation (QTM). Although ab initio calculations were performed for two families of compounds,

two groups introduced different models for the calculations. One group assumed four  $J_{\text{Fe–Dy}}$  are the same for compound **19**,<sup>[29]</sup> whereas the other group assumed there are two different  $J_{\text{Fe–Dy}}$  for four  $J_{\text{Fe–Dy}}$  in compounds **15**, **15 a**, **17**, **18** and **18 a**.<sup>[28]</sup> As shown in Table 2, they also used different spin Hamiltonian equations. This makes comparison tricky and thus a magnetostructural correlation impossible.

### 3.2.4.2. Change $\text{teaH}^-$ to $\text{thme}^{3-}$

It is also possible to obtain other  $\{\text{Fe}^{\text{III}}_2\text{Ln}^{\text{III}}\}$  butterfly CCs, in which the encapsulating ligand set differs from those discussed above. In this case the triol ligand, tris(hydroxymethyl)ethane ( $\text{thmeH}_3$ ) provides a different means of providing the central tribridging oxygen donors as well as further bridging between metal centres as shown in Figure 18a and 18a'. Thus the reaction of  $[\text{Fe}_3\text{O}(\text{O}_2\text{CPh})_6(\text{H}_2\text{O})_3](\text{NO}_3)$  with  $\text{Gd}(\text{NO}_3)_3 \cdot 6\text{H}_2\text{O}$  and  $\text{thmeH}_3$  in the presence of  $\text{Et}_3\text{N}$  in a 1:3:2:4 ratio in an acetonitrile/methanol (10:1) solvent mixture followed by slow evaporation led to the isolation of yellow crystals of  $[\text{NH}_4\text{Et}_3]_2[\text{Fe}^{\text{III}}_2\text{Gd}^{\text{III}}_2(\text{O}_2\text{Ph})_4(\text{thme})_2(\text{NO}_3)_4]$ . We note here the dianionic nature of the  $[\text{Fe}^{\text{III}}_2\text{Gd}^{\text{III}}_2(\text{O}_2\text{Ph})_4(\text{thme})_2(\text{NO}_3)_4]^{2-}$  coordination cluster core.



Table 2. The calculated J values for the {M<sup>III</sup><sub>2</sub>Dy<sub>2</sub>} butterflies.

		J <sup>tot</sup> <sub>3d-3d</sub>	J <sup>ex</sup> <sub>3d-3d</sub>	J <sup>dip</sup> <sub>3d-3d</sub>	J <sup>tot</sup> <sub>3d-Dy</sub>	J <sup>tot</sup> <sub>3d-Dy</sub>	J <sup>tot</sup> <sub>3d-Dy</sub>	J <sup>tot</sup> <sub>Dy-Dy</sub>	**J <sup>tot</sup> <sub>Dy-Dy</sub> <sup>(b)</sup>	J <sup>ex</sup> <sub>Dy-Dy</sub>	J <sup>dip</sup> <sub>Dy-Dy</sub>
[Fe <sup>III</sup> <sub>2</sub> Dy <sub>2</sub> (OH) <sub>2</sub> (teaH) <sub>2</sub> (p-CN-PhCO <sub>2</sub> ) <sub>6</sub> ] <b>18</b>	BS-DFT	-5.7			-0.12/-0.090			-0.0067	0.035	-0.18	0.53
	Fitted <sup>(a)</sup>	-5.7			-0.13/-0.090			-0.0067			
[Fe <sup>III</sup> <sub>2</sub> Dy <sub>2</sub> (OH) <sub>2</sub> (teaH) <sub>2</sub> (m-Me-PhCO <sub>2</sub> ) <sub>6</sub> ] <b>15a</b>	BS-DFT	-8.2			-0.21/-0.046			-0.011	-0.02	-0.50	0.48
	Fitted <sup>(a)</sup>	-21.0 (-10*)			-0.30 (0.17*)/ -0.01 (-0.10*)			-0.011 (-0.02*)			
[Fe <sup>III</sup> <sub>2</sub> Dy <sub>2</sub> (OH) <sub>2</sub> (teaH) <sub>2</sub> (m-CN-PhCO <sub>2</sub> ) <sub>6</sub> ] <b>18a</b>	BS-DFT	-8.6			-0.31/-0.17			-0.024	-0.03	-0.60	0.57
	Fitted <sup>(a)</sup>	-8.6			-0.31/-0.17			-0.024			
[Fe <sup>III</sup> <sub>2</sub> Dy <sub>2</sub> (OH) <sub>2</sub> (teaH) <sub>2</sub> (p-NO <sub>2</sub> -PhCO <sub>2</sub> ) <sub>6</sub> ] <b>17</b>	BS-DFT	-6.3			-0.088/-0.11			0	0.61	0	0.61
	Fitted <sup>(a)</sup>	-6.3			-0.005/ -0.005			0			
	BS-DFT	-8.8			-0.26/-0.26			-0.011	0.65	0	0.65
[Fe <sup>III</sup> <sub>2</sub> Dy <sub>2</sub> (OH) <sub>2</sub> (teaH) <sub>2</sub> (p-Me-PhCO <sub>2</sub> ) <sub>6</sub> ] <b>15</b>	Fitted	-14.0 (-9.5*)			-0.26 (0.20*)/ -0.27 (-0.20*)			-0.010 (0*)			
		J <sup>tot</sup> <sub>3d-3d</sub>	J <sup>ex</sup> <sub>3d-3d</sub>	J <sup>dip</sup> <sub>3d-3d</sub>	J <sup>tot</sup> <sub>3d-Dy</sub>	J <sup>tot</sup> <sub>3d-Dy</sub>	J <sup>tot</sup> <sub>3d-Dy</sub>	J <sup>tot</sup> <sub>Dy-Dy</sub>	J <sup>ex</sup> <sub>Dy-Dy</sub>	J <sup>dip</sup> <sub>Dy-Dy</sub>	ZJ
[Cr <sup>III</sup> <sub>2</sub> Dy <sub>2</sub> (OH) <sub>2</sub> (pmide) <sub>2</sub> (p-Me-PhCO <sub>2</sub> ) <sub>6</sub> ] <b>19b</b>	Fitted <sup>(c)</sup>	-0.65	-0.50	-0.15	-1.15	-0.80	-0.35	0.405	0.370	0.035	-0.045
[Mn <sup>III</sup> <sub>2</sub> Dy <sub>2</sub> (OH) <sub>2</sub> (pmide) <sub>2</sub> (p-Me-PhCO <sub>2</sub> ) <sub>6</sub> ] <b>19c</b>	Fitted <sup>(d)</sup>	-3.20	-2.10	-1.10	0.15	0.09	0.06	0.035	-0.001	0.036	-
[Fe <sup>III</sup> <sub>2</sub> Dy <sub>2</sub> (OH) <sub>2</sub> (pmide) <sub>2</sub> (p-Me-PhCO <sub>2</sub> ) <sub>6</sub> ] <b>19</b>	Fitted <sup>(e)</sup>	-4.20	-3.00	-1.20	-0.12	-0.05	-0.07	-0.060	0.025	0.035	-
[Al <sup>III</sup> <sub>2</sub> Dy <sub>2</sub> (OH) <sub>2</sub> (pmide) <sub>2</sub> (p-Me-PhCO <sub>2</sub> ) <sub>6</sub> ] <b>21a</b>	Fitted <sup>(f)</sup>	-	-	-	-	-	-	0.049	0.025	0.024	-

\*A small rescaling of the experimental data is in principle justified given the possible experimental errors due to the absorption of solvent molecules or mass error.  
\*\*Magnetic interactions between Dy<sup>III</sup> corresponding to pseudospin of 1/2 of the ground KDs on the dysprosium sites.

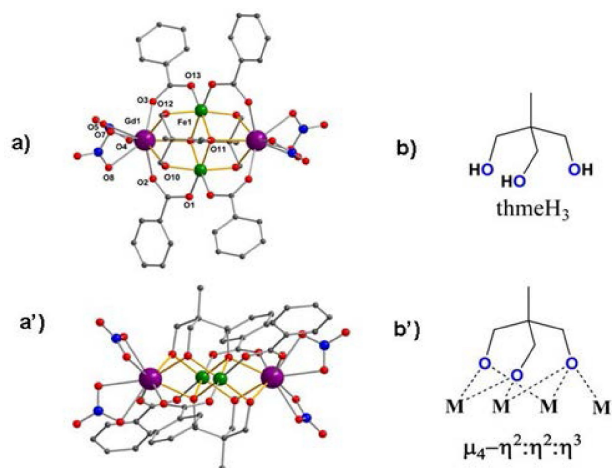


Figure 18. The structure of [Fe<sup>III</sup><sub>2</sub>Gd<sup>III</sup><sub>2</sub>(thme)<sub>2</sub>(PhCO<sub>2</sub>)<sub>4</sub>(NO<sub>3</sub>)<sub>4</sub>], **22** (a) and side view (a'); the coordination thmeH<sub>3</sub> ligands (b) and the coordination mode of thmeH<sub>3</sub> (b'). Adapted with permission from Ref. [22] Copyright 2010, Elsevier.

$$\begin{aligned}
 \text{a) } \hat{H} = & -J_{Dy1-Dy1'} S_{Dy1} S_{Dy1'} - J_{Dy1-Fe1} (S_{Dy1} S_{Fe1} + S_{Dy1'} S_{Fe1'}) \\
 & - J_{Dy1-Fe1'} (S_{Dy1} S_{Fe1'} + S_{Dy1'} S_{Fe1}) - J_{Fe1-Fe1'} S_{Fe1} S_{Fe1'}
 \end{aligned} \quad (1)$$

$$S_{Dy} = 5/2 \text{ and } S_{Fe} = 5/2, J^{tot} = J^{ex} + J^{dip}$$

$$\text{b) } \hat{H} = -J_{Dy-Dy}^{tot} \hat{S}_{Dy1} \hat{S}_{Dy2} \quad (2)$$

$$\hat{S}_{Dy} = 1/2, J^{tot} = J^{ising} + J^{dip}$$

$$\begin{aligned}
 \text{c) } \hat{H} = & -J_{Dy1-Dy2}^{tot} \hat{S}_{Dy1} \hat{S}_{Dy2} - J_{Dy-Cr}^{tot} \\
 & (\hat{S}_{Dy1} \hat{S}_{Cr1} + \hat{S}_{Dy1} \hat{S}_{Cr2} + \hat{S}_{Dy2} \hat{S}_{Cr1} + \hat{S}_{Dy2} \hat{S}_{Cr2}) \\
 & - J_{Cr-Cr}^{tot} \hat{S}_{Cr1} \hat{S}_{Cr2}
 \end{aligned} \quad (3)$$

$$\hat{S}_{Dy} = 1/2, \hat{S}_{Cr} = 3/2, J^{tot} = J^{ex} + J^{dip}$$

$$\begin{aligned}
 \text{d) } \hat{H} = & -J_{Dy1-Dy2}^{tot} \hat{S}_{Dy1} \hat{S}_{Dy2} - J_{Dy-Mn}^{tot} \\
 & (\hat{S}_{Dy1} \hat{S}_{Mn1} + \hat{S}_{Dy1} \hat{S}_{Mn2} + \hat{S}_{Dy2} \hat{S}_{Mn1} + \hat{S}_{Dy2} \hat{S}_{Mn2}) \\
 & - J_{Mn-Mn}^{tot} \hat{S}_{Mn1} \hat{S}_{Mn2}
 \end{aligned} \quad (4)$$

$$\hat{S}_{Dy} = 1/2, \hat{S}_{Mn} = 5/2, J^{tot} = J^{ex} + J^{dip}$$

$$\begin{aligned}
 \text{e) } \hat{H} = & -J_{Dy1-Dy2}^{tot} \hat{S}_{Dy1} \hat{S}_{Dy2} - J_{Dy-Fe}^{tot} \\
 & (\hat{S}_{Dy1} \hat{S}_{Fe1} + \hat{S}_{Dy1} \hat{S}_{Fe2} + \hat{S}_{Dy2} \hat{S}_{Fe1} + \hat{S}_{Dy2} \hat{S}_{Fe2}) \\
 & - J_{Fe-Fe}^{tot} \hat{S}_{Fe1} \hat{S}_{Fe2}
 \end{aligned} \quad (5)$$

$$\hat{S}_{Dy} = 1/2, \hat{S}_{Fe} = 5/2, J^{tot} = J^{ex} + J^{dip}$$

$$\text{f) } \hat{H} = -J_{Dy-Dy}^{tot} \hat{S}_{Dy1} \hat{S}_{Dy2} \quad (6)$$

$$\hat{S}_{Dy} = 1/2, J^{tot} = J^{ex} + J^{dip}$$

Compound **22** crystallises in the monoclinic space group P2<sub>1</sub>/n with the coordination cluster core lying on an inversion centre. The planar {Fe<sup>III</sup><sub>2</sub>Gd<sub>2</sub>} butterfly core topology has the Type I arrangement with the Fe<sub>2</sub> centres in the body positions. In this case, the μ<sub>2</sub>-O and μ<sub>3</sub>-O bridging oxygens are provided by deprotonated alkoxide arms of two thme<sup>3-</sup> ligands each

binding in the  $\mu_4\text{-}\eta^2\text{:}\eta^2\text{:}\eta^3$  bridging mode (Figure 18b'). The pairs of  $\{\text{Fe}^{\text{III}}\text{Gd}\}$  units are bridged by four  $\eta^1\text{:}\eta^1\text{:}\mu_2\text{-O}_2\text{CPh}$  ligands. There are also two chelating co-ligand nitrate ions on each wingtip Gd<sup>III</sup> ion. The body Fe<sup>III</sup> ions are both six-coordinate with distorted octahedral (OC-6) geometries, while the Gd<sup>III</sup> ions are both nine-coordinate with distorted muffin (MFF-9) geometries. (See Table 1).

Dc magnetic susceptibility studies indicated dominant antiferromagnetic interactions in **22**. The experimental  $\chi T$  versus T data in Figure 19 as a function of two exchange parameters  $J_1$  (Fe<sup>III</sup>–Fe<sup>III</sup> interaction) and  $J_2$  (Fe<sup>III</sup>–Gd<sup>III</sup> interactions) was modelled using an isotropic Kambe vector coupling method.<sup>[31]</sup> A satisfactory fit could be obtained using the assumption that the Fe<sup>III</sup>–Gd<sup>III</sup> coupling is negligible and  $J_2$  was set to zero, giving  $J_1 = -3.4$  (1) cm<sup>-1</sup> and  $g = 2.07$  (5). These parameters are smaller than those found for compound **9**  $\{\text{Fe}^{\text{III}}_2\text{Gd}_2\}$ , for which the  $J_{\text{Fe-Fe}}$ ,  $J_{\text{Fe-Gd}}$  and  $g$  are  $-6.71$  (4) cm<sup>-1</sup>,  $+0.18$  (1) cm<sup>-1</sup> and 2.0, respectively. These differences underline the important steering effect changes in the encapsulating ligand fields can have on the details of the magnetic properties of the butterfly cores.

### 3.3. The case of $\{\text{Fe}^{\text{III}}_2\text{Ln}_2\}$ butterflies which can be Type I or Type II

#### 3.3.1. Body/wing swapping within a set of synthetic variables

It is of interest to speculate what directs whether the 3d metal ions occupy the body or wing-tip positions. As was mentioned in the introductory section, the butterflies produced in the Murray group<sup>[6c]</sup> usually have the Type II arrangement (3d metal ions in wing-tips) whereas most other examples have the Type I arrangement with the 3d metal ions in the body positions.

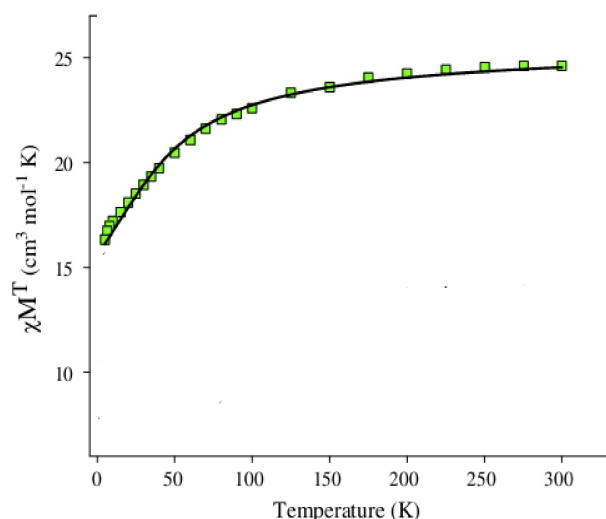


**Figure 19.**  $\chi T$  versus T plot for complex **22** in the temperature range 5.0–300 K in 0.1 T applied dc field. The solid lines are fits to the experimental using the Kambe vector coupling method.<sup>[31]</sup> Adapted with permission from Ref. [22] Copyright 2010, Elsevier.

We found that careful control of the reaction conditions for the system Fe<sup>III</sup>/Ln<sup>III</sup>/H<sub>2</sub>teg/pivalic acid allowed for the isolation of two different series butterfly coordination clusters with the formulation  $[\text{Fe}^{\text{III}}_2\text{Ln}_2(\mu_3\text{-OH})_2(\text{teg})_2(\text{N}_3)_2(\text{piv})_4]$  where Ln=Y (**23**), Dy (**24**) and Ho (**25**) and  $[\text{Fe}^{\text{III}}_2\text{Ln}_2(\mu_3\text{-MeO})_2(\text{teg})_2(\text{NO}_3)_2(\text{piv})_4]$  where Ln=Y (**26**), Dy (**27**) and Ho (**28**). In the first series the Fe<sup>III</sup> centres occupy the wingtip positions, leading to the Type II arrangement, which is the first observation of this topology for  $\{\text{Fe}^{\text{III}}_2\text{Ln}_2\}$  butterflies. In the second series, the cores are of Type I with the Ln<sup>III</sup> ions in the wing-tip positions (Figure 20).

The main difference in the synthetic procedure for these compounds was that compounds **23–25** were synthesised in MeCN with azide present whereas **26–28** were crystallised from MeOH–MeCN mixtures. The two sets of compounds crystallise in isostructural series. Thus, the crystal structures of **23** and **26** were described to reveal the structural features. The  $\{\text{Fe}^{\text{III}}_2\text{Ln}_2\}$  cores for both types are held together by two  $\mu_3$ -oxygen atoms which for **23–25** come from two OH<sup>-</sup> ions and for **26–28** from two MeO<sup>-</sup> groups. For both sets of complexes, the two doubly deprotonated teg<sup>2-</sup> ligands display the same  $\mu_3\text{:}\eta^2\text{:}\eta^1\text{:}\eta^1\text{:}\eta^2$  coordination geometry, chelating Dy<sup>III</sup> ions with their O4 donors and bridging two Fe<sup>III</sup> ions with deprotonated alcohol arms, respectively and each of the four pivalic acid bridge one Fe<sup>III</sup> ion and one Dy<sup>III</sup> ion. The outer co-ligands of **23–25** are two azides coordinating to the wingtip Fe<sup>III</sup> ions, while for **26–28**, there are two NO<sub>3</sub><sup>-</sup> co-ligands chelated to the wingtip Dy<sup>III</sup> ions. The eight coordinate Ln<sup>III</sup> ions in **23–25** have dodecahedral and the nine coordinate ions in **26–28** capped square anti-prismatic coordination geometries.

All Fe ions adopt essentially octahedral coordination geometry. It is interesting to speculate what influences where the 3d and 4f metal ions go in terms of the body versus wingtip positions. In the case of these two systems, we can note that the iron starting materials were simple salts rather

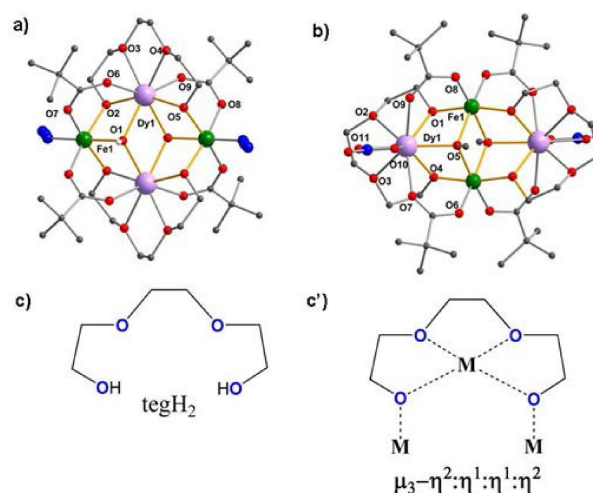


**Figure 20.** The structures of  $[\text{Fe}^{\text{III}}_2\text{Dy}_2(\mu_3\text{-OH})_2(\text{teg})_2(\text{N}_3)_2(\text{piv})_4]$ , **24** with azide ligands (a) and  $[\text{Fe}^{\text{III}}_2\text{Dy}^{\text{III}}_2(\mu_3\text{-MeO})_2(\text{teg})_2(\text{NO}_3)_2(\text{piv})_4]$  **27** (b). H atoms of C atoms are omitted for clarity. Colour code Fe (green), Dy (purple), O (red), C (grey), N (blue); the coordination  $\text{tegH}_2$  ligands (c) and the coordination mode of  $\text{tegH}_2$  (c') Reprinted with permission from Ref. [23] Copyright 2013, The Royal Society of Chemistry.

than carboxylate triangles. This gives the system more freedom and presumably the self-assembly process is the deciding factor here.

For both sets of compounds dominant antiferromagnetic interactions are present between paramagnetic centres as expected and shown for  $\{\text{Fe}^{\text{III}}_2\text{Ln}_2\}$  systems in other studies (Figure 21). It can be seen from a comparison of the data for the two systems that the strong antiferromagnetic interactions between the body iron centres in **26–28** result in a greater decrease in the dc susceptibilities. The ac susceptibility measurements revealed no out-of-phase signals could be observed for all the compounds above 1.8 K.

For the first time, a change in synthetic procedure resulted in a different arrangement of the relative positions of the  $\text{Fe}^{\text{III}}$  ions and  $\text{Ln}^{\text{III}}$  ions within an Fe-4f butterfly. This offers a means to steer the structural and electronic features within a 3d-4f system within the same ligand shell. Compounds **23–25** are the only reported  $\{\text{Fe}^{\text{III}}_2\text{Ln}_2\}$  CCs where the  $\text{Ln}^{\text{III}}$  ions occupy the body positions.

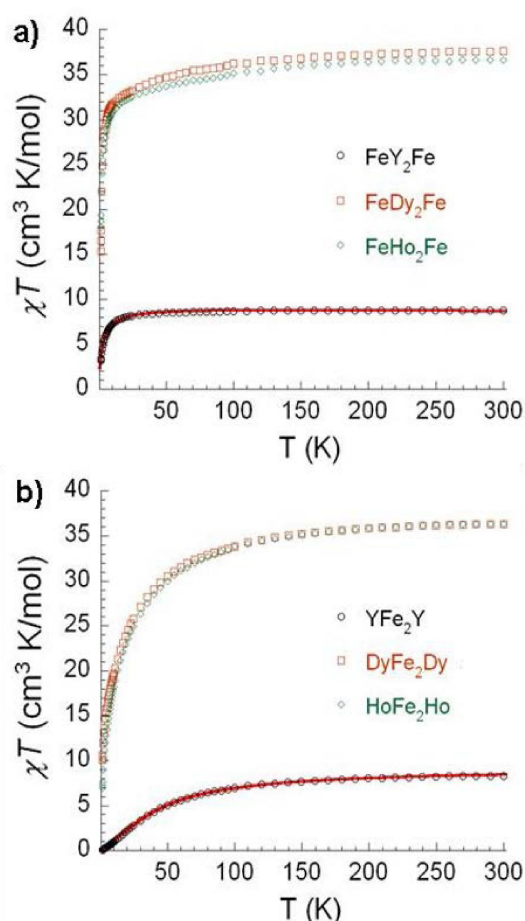


**Figure 21.** Temperature dependence of the  $\chi T$  products under 1000 Oe or compounds **23–25** (top) and **26–28** (bottom); The solid line represents the Curie-Weiss fit for compound **23** and the best fit for compound **26** using a dimeric model of  $S = 5/2$ . Reprinted with permission from Ref. [23] Copyright 2013, The Royal Society of Chemistry.

### 3.3.2. Co-ligand variation for the Type II $[\text{Fe}^{\text{III}}_2\text{Ln}_2(\text{OH})_2(\text{teg})_2(\text{N}_3)_2(\text{RCO}_2)_4]$ compounds

In order to investigate whether changing the nature of the bridging carboxylate might alter the behaviour of the Type II  $[\text{Fe}^{\text{III}}_2\text{Ln}_2(\mu_3\text{-OH})_2(\text{teg})_2(\text{N}_3)_2(\text{Me}_3\text{CCO}_2)_4]$  system where the  $\text{Fe}^{\text{III}}$  ions are in the wingtip positions, the analogues  $[\text{Fe}^{\text{III}}_2\text{Ln}_2(\mu_3\text{-OH})_2(\text{teg})_2(\text{N}_3)_2(\text{PhCO}_2)_4]$ ,  $\text{Ln} = \text{Y}$  (**29**) and  $\text{Dy}$  (**30**) were produced, in which the pivalate,  $\text{Me}_3\text{CCO}_2^-$ , co-ligand is changed to benzoate (Figure 22a).<sup>[24]</sup>

Magnetic measurements on both compounds revealed dominant antiferromagnetic interactions between the metal centres (Figure 22b). The ac susceptibilities measurement indicates compound **30** show slow relaxation of the magnetisation, but without maxima above 1.8 K even at 1500 Hz (Figure 23). This suggested that the replacement of pivalate with benzoate slows down the relaxation of  $\{\text{Fe}^{\text{III}}_2\text{Dy}_2\}$ , is consistent with the  $\{\text{Fe}^{\text{III}}_2\text{Dy}^{\text{III}}_2\}$  with  $\text{Fe}^{\text{III}}$  ions in body.

The  $^{57}\text{Fe}$  Mössbauer spectra complement the ac magnetic susceptibility measurements, which show a static magnetic field can quench the slow relaxation of magnetisation generated by the anisotropic  $\text{Dy}^{\text{III}}$  ions (Figure 24). This was shown by studying the  $\{\text{FeY}_2\text{Fe}\}$  analogue **29** which at 3 K in zero applied external field shows an asymmetric doublet typical for octahedrally coordinated high-spin  $\text{Fe}^{\text{III}}$  ions with paramagnetic relaxation times near the typical time window of Mössbauer spectroscopy of about  $10^{-7}$  s (Figure 24, top). The fact that the iron centres are approximately 5.5 Å apart means that these are essentially independent. On the other hand, compound **30**, the  $\{\text{FeDy}_2\text{Fe}\}$  analogue, shows a well-defined magnetic sextet at  $T = 3$  K with zero external field (Figure 24, bottom). The fact that the Mössbauer pattern of **30** obtained at  $T = 30$  K (Figure 24, bottom) resembles that observed for **29** at  $T = 3$  K (Figure 24, top). Given the  $10^{-7}$  s time window of Mössbauer spectroscopy, the ferric high-spin  $\text{Fe}^{\text{III}}$  ions in **30** must relax with a relaxation rate much smaller than  $10^{-7}$  s and it was concluded that the presence of paramagnetic  $\text{Dy}^{\text{III}}$  ions cause a significant decrease in the iron spin-spin relaxation rate from much more than  $10^{-7}$  s in the  $\text{Y}^{\text{III}}$  complex **29** to much less than  $10^{-7}$  s in the  $\text{Dy}^{\text{III}}$  complex **30**.

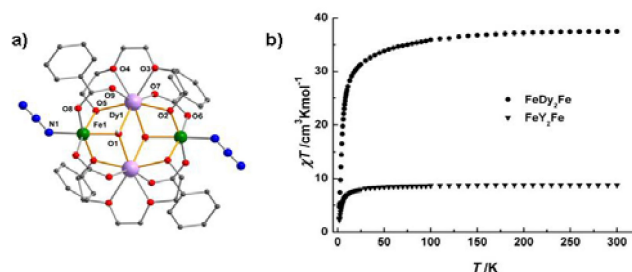


**Figure 22.** Molecular structure of compound  $[\text{Fe}^{\text{III}}_2\text{Dy}_2(\mu_3\text{-OH})_2(\text{teg})_2(\text{N}_3)_2(\text{PhCO}_2)_4]$ , **30**, (a). H atoms on carbon atoms are omitted for clarity. The  $\chi T$  versus  $T$  plots for compounds **29** and **30** at 1000 Oe (b). Reproduced with permission from Ref. [24] Copyright 2015, Wiley-VCH.

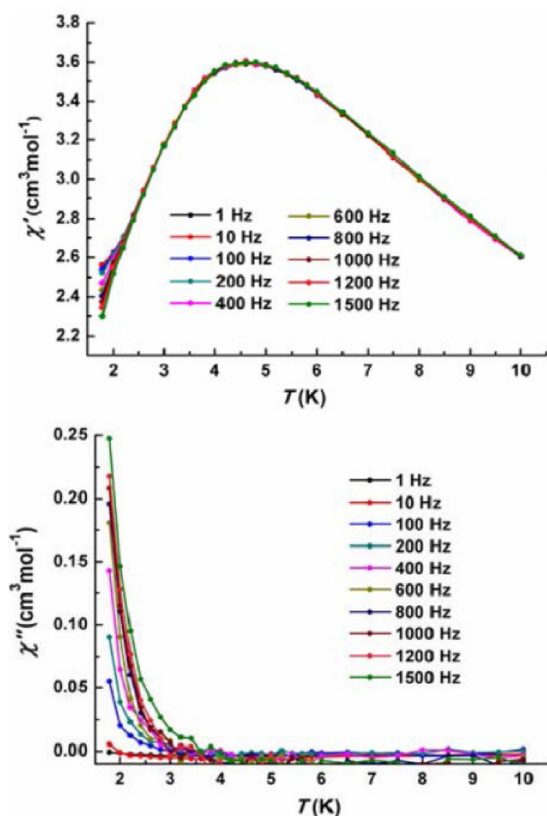


**Figure 23.** Temperature dependence of in-phase and out-of-phase ac magnetic susceptibility under zero-dc field for compound **29**. Reproduced with permission from Ref. [24] Copyright 2015, Wiley-VCH.

### 3.3.3. Changing the ratios in mixed ligand/co-ligand sets

In  $[\text{Fe}^{\text{III}}_2\text{Ln}_2(\text{OH})_2(\text{dda})_2(\text{fpdH})_2(\text{NO}_3)_4(\text{H}_2\text{O})_{1.5}(\text{MeOH})_{0.5}] \cdot 6\text{MeCN}$  (Figure 25a) the compounds with  $\text{Ln}=\text{Y}$  (**31**) and  $\text{Dy}$  (**32**) could be obtained. Here,  $\text{ddaH}_2$  is 2,3-dihydroxybenzaldehyde and  $\text{fpdH}_2$  is the Schiff base of this aldehyde with furfurylamine, which forms in situ during the synthesis (see Figure 25b and c). The compounds were made by mixing  $\text{Fe}^{\text{III}}(\text{ClO}_4)_2 \cdot 6\text{H}_2\text{O}$ ,  $\text{Ln}^{\text{III}}(\text{NO}_3)_3 \cdot 6\text{H}_2\text{O}$ , 2,3-dihydroxybenzaldehyde ( $\text{ddaH}_2$ ), furfurylamine, and triethylamine in the molar ratio 1:1:1:1:1 in MeOH/MeCN and crystallise in the monoclinic space group  $P2_1/n$  with the cores sitting on an inversion centre. The planar  $\{\text{Fe}^{\text{III}}_2\text{Ln}_2\}$  butterfly core is of Type I with the  $\text{Fe}^{\text{III}}$  ions in the body positions.<sup>[32]</sup> The two  $\mu_3\text{-O}$  ligands of the central core are provided by hydroxides likely deriving from water molecules in the reaction mixture, whereas the four bridging  $\mu_2\text{-O}$  ligands of the core are provided by phenolate oxygens from the benzaldehyde groups. Thus, two doubly-deprotonated dihydroxy benzaldehyde ( $\text{dda}^{2-}$ ) ligands displaying  $\mu_2\text{-}\eta^1:\eta^2:\eta^1$  Figure 25b and b') coordination geometry and two doubly-deprotonated Schiff-base ( $\text{pfd}^{2-}$ ) ligands displaying  $\mu_2\text{-}\eta^1:\eta^2:\eta^0:\eta^0$  Figure 25c and c') coordination geometry chelate and bridge the metal ions, taking over the role of both the main ligand (in comparison with, for example, the role of the deprotonated arms of the triethanolamine ligands described for

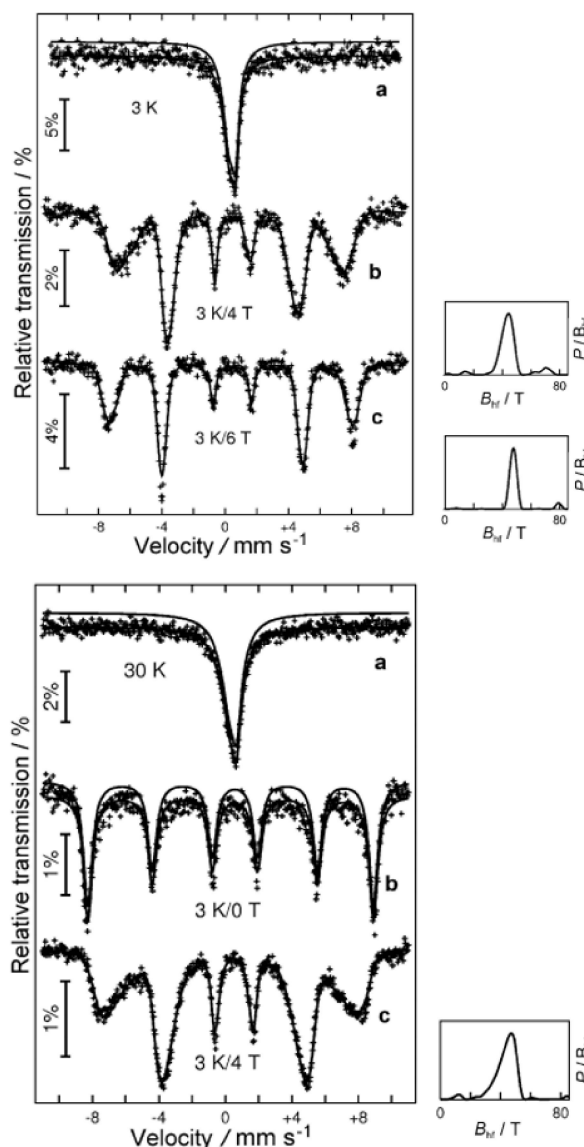


**Figure 24.**  $^{57}\text{Fe}$  Mössbauer spectra of **29**  $[\text{Fe}^{\text{III}}_2\text{Dy}_2]$  at 30 K and 3 K in zero field and applied external magnetic field (top) and  $^{57}\text{Fe}$  Mössbauer spectra of **30**  $[\text{Fe}^{\text{III}}_2\text{Y}_2]$  at 3 K in zero field and applied external magnetic fields (right). Reproduced with permission from Ref. [24] Copyright 2015, Wiley-VCH.

compound **3**) as well as the role of the bridging co-ligands. Because this involves fewer donors being available for the wing-tip lanthanides, extra peripheral ligation to the two  $\text{Y}^{\text{III}}$  or  $\text{Dy}^{\text{III}}$  ions is provided by four chelating nitrate ions and two water molecules, that is, two chelating nitrates and an aqua ligand per  $\text{Ln}^{\text{III}}$  centre. The  $\text{Fe}^{\text{III}}$  are six coordinate with OC-6 geometry and the  $\text{Ln}^{\text{III}}$  ions nine-coordinate with CSAPR-9 coordination geometry.

The dc susceptibilities measurement for compounds **31** and **32** indicates dominant antiferromagnetic  $\text{Fe}^{\text{III}}\text{--Fe}^{\text{III}}$  interaction in **31**, which is consistent with the reported  $\{\text{Fe}^{\text{III}}_2\text{Y}_2\}$  compounds but dominant ferromagnetic interaction in **32** (Figure 26). Furthermore, the best fit to the  $\chi T$  versus  $T$  curve for compound **31** according to the Hamiltonian  $H = -2J_1S_1S_2$  equation gave  $g =$



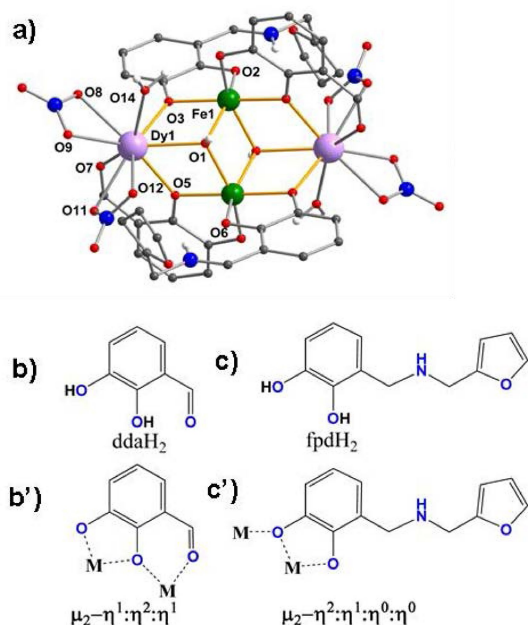


**Figure 25.** Molecular structure of  $[\text{Fe}^{\text{III}}_2\text{Ln}_2(\mu_3\text{-OH})_2(\text{dda})_2(\text{fpdH})_2(\text{NO}_3)_4(\text{H}_2\text{O})_2]$ , **32** (organic H atoms and the minor MeOH component of the terminal ligand on Ln (1) are omitted for clarity; O red; N blue; C black; H white). Reprinted with permission from Ref. [32] Copyright 2013, The Royal Society of Chemistry.

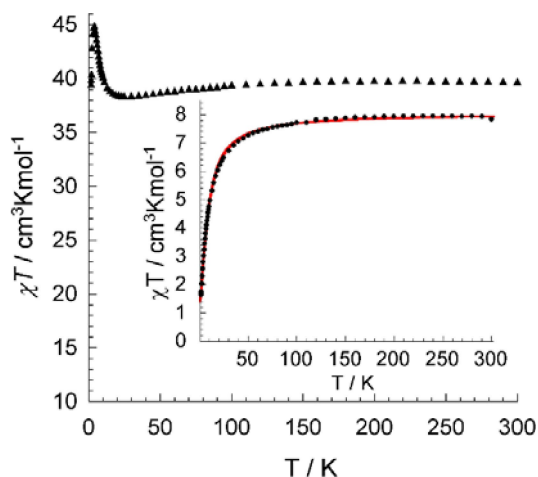


**Figure 26.**  $\chi T$  vs.  $T$  plots at 1000 Oe for **32** and  $\chi T$  vs.  $T$  plots at 1000 Oe for **31** (inset). The solid line is the best fit to the experimental data. Reprinted with permission from Ref. [32] Copyright 2013, The Royal Society of Chemistry.

1.92(1) and an exchange parameter  $J_{\text{Fe-Fe}} = -0.46$  (1)  $\text{cm}^{-1}$ , which is smaller than the reported  $J_{\text{Fe-Fe}}$  values for all previously reported dinuclear  $\{\text{Fe}^{\text{III}}_2(\mu\text{-OH})_2\}$  compounds, for which the smallest reported so far was  $-2.1$   $\text{cm}^{-1}$  for a complex with five-coordinate  $\text{Fe}^{\text{III}}$  centres. The results revealed that it was necessary to apply an external field to overcome the Fe–Fe antiferromagnetic coupling in the  $\{\text{Fe}^{\text{III}}_2\text{Y}_2\}$  compound **31**. This reorientates the  $\text{Fe}^{\text{III}}$  moments into a parallel (ferromagnetic) spin arrangement. On the other hand, the intramolecular

magnetic field generated by the anisotropic  $\text{Dy}^{\text{III}}$  ions in the  $\{\text{Fe}^{\text{III}}_2\text{Dy}_2\}$  compound **32** is already sufficient to overcome the Fe–Fe antiferromagnetic coupling to give the ferromagnetic spin orientation (Figure 27).

No out-of-phase signal was observed in the ac susceptibility measurements for compound **31** as would be expected. For compound **32**, out-of-phase ac signals were observed (Figure 28), but without maximum even under applied dc field. 4. Concluding Remarks and Outlook

Results achieved on  $\{\text{Fe}^{\text{III}}_2\text{Ln}_2\}$  butterfly CCs in the last few years show that this provides an excellent “test-bed” system to allow for the investigation of fine-tuning effects introduced through variations in the ligand shell as well as in the nature of the 4f ion. Clearly, up to now not all aspects have been

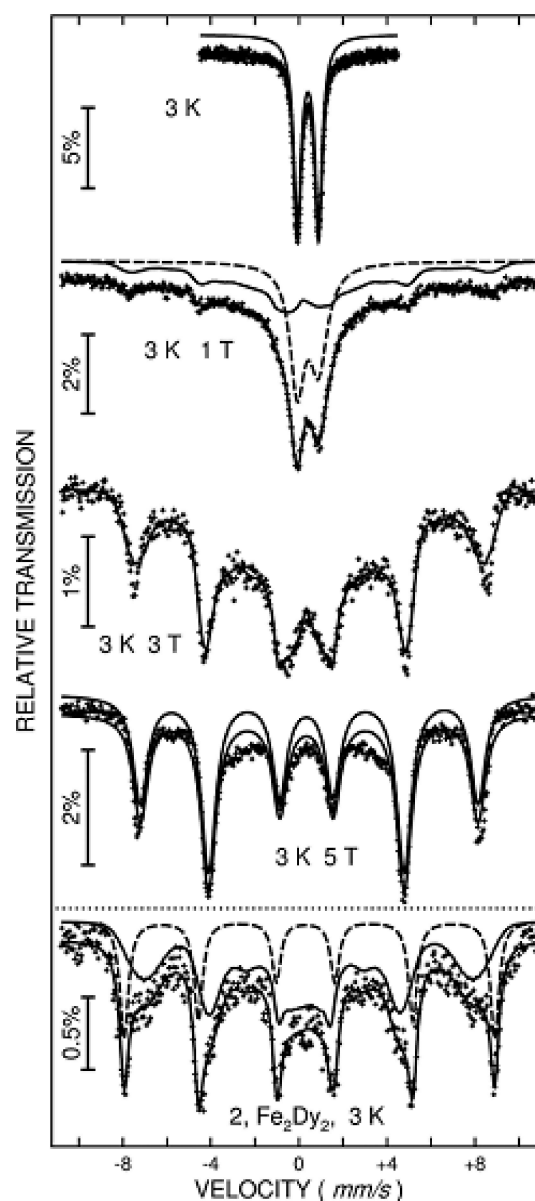


**Figure 27.** Plots of in-phase (left) and out-of-phase (right) ac susceptibility signals vs. temperature for **32** ( $\text{Fe}^{\text{III}}_2\text{Dy}_2$ ) under zero dc field. Reprinted with permission from Ref. [32] Copyright 2013, The Royal Society of Chemistry.



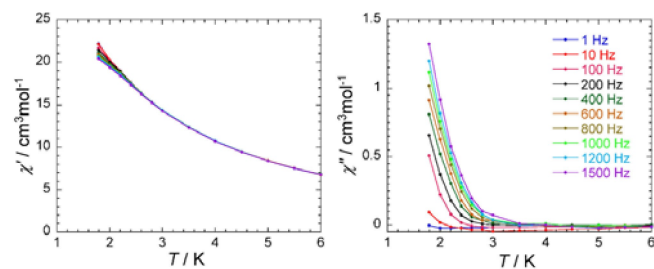


**Figure 28.**  $^{57}\text{Fe}$  Mössbauer spectra for **31** at 3 K in zero- and applied external magnetic fields; Bottom: spectrum for **32** at 3 K in zero external magnetic fields given for comparison. Reprinted with permission from Ref. [32] Copyright 2013, The Royal Society of Chemistry.

investigated in depth, for example, there are only sparse reports on series of compounds where only the 4f ion is varied. For the variables within the ligand shells, it has proved possible to study rather subtle changes on parts of the ligand which are remote from the cluster core. These reveal some dramatic differences in the electronic and magnetic structures of the cores as could be revealed, for example, using Mössbauer spectroscopy. In this case, the choice of  $\{\text{Fe}^{\text{III}}_2\text{Ln}_2\}$  butterflies have allowed for the sensitive Mössbauer effect to be used as a tool to study the effects on the  $^{57}\text{Fe}$  nucleus. This is a useful adjunct to the more standard techniques, such as bulk susceptibility studies, which are generally used to characterise molecular magnets. Furthermore, the fact that the Mössbauer measurements take place in a different timescale regime from that of ac susceptibility measurements gives a further handle on exploring relaxation effects in these systems.

Further twists on the story are provided by varying the nature of the encapsulating ligands as well as varying the synthetic procedures. This can lead to changing the relative positions of the metal centres and also introduce the possibility of observing multiple relaxation events.

In terms of the outlooks such studies can provide, one observation is that very often  $\text{Dy}^{\text{III}}$  is the best choice of 4f ion to incorporate in these systems. This is in line with the results of the very many studies on  $\text{Dy}^{\text{III}}$  containing SMMs in general. A more surprising observation concerns the fine-tuning which the encapsulating ligands provide. A simple example was provided by changing substituents on the carboxylate co-ligands. It was also noted that changes to the chelating ligands and co-ligands on the 4f ion can influence the relaxation behaviour. Obviously, there are many further systems to tune in these ways. One aspect which has hardly been explored is that of tuning via changes in the substituent on the  $\mu_3$ -OR bridging moieties of the butterfly core. Furthermore, systematic studies on varying the 3d metal ions should also be undertaken. Although aminoalcohol ligands in the context of the butterfly systems rarely produce spectacular single-molecule magnet properties these ligands have been used in cyclic systems such as  $\text{Fe}_4\text{Dy}_4$  (SMM),<sup>[33]</sup>  $\text{Fe}_{16}\text{Ln}_4$  (exotic spin structures),<sup>[34]</sup>  $\text{Fe}_{10}\text{Ln}_{10}$  (high spin systems showing properties such as quantum critical point<sup>[35]</sup> and exciton formation<sup>[36]</sup>) and  $\text{Fe}_{18}\text{Dy}_6$  (giant toroidal moment).<sup>[37]</sup>

In conclusion, the butterfly system can provide a huge number of magnetically interesting systems whose properties can be fine-tuned according to potential applications.

## Abbreviations

SMM	Single molecule magnet
SIM	Single ion magnet
QTM	Quantum tunnelling of magnetisation
ZFQTM	Zero field quantum tunnelling
TAQTM	Thermally assisted quantum tunnelling
ZFS	Zero field splitting
EPR	Electron Paramagnetic Resonance
POM	Polyoxometalate
CCs	Coordination clusters
LF	Ligand field
CF	Crystal field
SAP	Square antiprismatic
OC	Octahedron
TDD	Triangular Dodecahedron
JSD	Snub Disphenoid
BTPR	Biaugmented Trigonal Prism
JCSAPR	Capped square antiprism J10
CSAPR	Capped Square antiprism
TCTPR	Tricapped trigonal prism
MFF	Muffin
teaH <sub>3</sub>	Triethanolamine
pmideH <sub>2</sub>	2,2'-((pyridin-2-ylmethyl)azanediyl)bis(ethan-1-ol)
thmeH <sub>3</sub>	2-(hydroxymethyl)-2-methylpropane-1,3-diol
tegH <sub>2</sub>	2,2'-(ethane-1,2-diylbis(oxy))bis(ethan-1-ol)
ddaH <sub>2</sub>	2,3-dihydroxybenzaldehyde
pdfH <sub>2</sub>	3-(((furan-2-ylmethyl)amino)methyl)benzene-1,2-diol

## Acknowledgements

We gratefully acknowledge financial support from the DFG SFB/TRR88 "3MET". We also acknowledge the many contributions from other members of the research group who have been active in this area. Their results are discussed here within the context of the international efforts on Fe-4f butterflies. We thank Dr. Rouven F. Pflieger for providing the picture for the frontispiece. Open Access funding enabled and organized by Projekt DEAL.

## Conflict of Interest

The authors declare no conflict of interest.

**Keywords:** cooperativity · Iron · lanthanides · Mössbauer spectroscopy · molecular magnetism

[1] J. Long, F. Habib, P.-H. Lin, I. Korobkov, G. Enright, L. Ungur, W. Wernsdorfer, L. F. Chibotaru, M. Murugesu, *J. Am. Chem. Soc.* **2011**, *133*, 5319–5328.

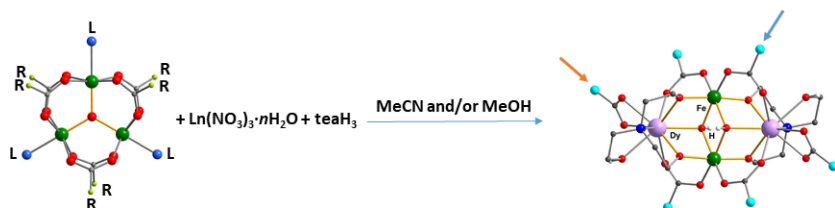
- [2] Z.-S. Meng, F.-S. Guo, J.-L. Liu, J.-D. Leng, M.-L. Tong, *Dalton Trans.* **2012**, 41, 2320–2329.
- [3] S. M. T. Abtab, M. Maity, K. Bhattacharya, E. C. Sañudo, M. Chaudhury, *Inorg. Chem.* **2012**, *51*, 10211–10221.
- [4] N. F. Chilton, S. K. Langley, B. Moubaraki, K. S. Murray, *Chem. Commun.* **2010**, *46*, 7787–7789.
- [5] H. L. C. Feltham, R. Clérac, L. Ungur, L. F. Chibotaru, A. K. Powell, S. Brooker, *Inorg. Chem.* **2013**, *52*, 3236–3240.
- [6] a) V. Chandrasekhar, P. Bag, M. Speldrich, J. van Leusen, P. Kögerler, *Inorg. Chem.* **2013**, *52*, 5035–5044; b) J.-P. Costes, M. Auchel, F. Dahan, V. Peyrou, S. Shova, W. Wernsdorfer, *Inorg. Chem.* **2006**, *45*, 1924–1934; c) K. S. Murray, *Adv. Inorg. Chem.*, Vol. 43 (Ed.: A. G. Sykes), Academic Press **1995**, pp. 261–358.
- [7] Z. E. Serna, M. K. Uriaga, M. G. Barandika, R. Cortés, S. Martín, L. Lezama, M. I. Arriortua, T. Rojo, *Inorg. Chem.* **2001**, *40*, 4550–4555.
- [8] P.-H. Lin, T. J. Burchell, L. Ungur, L. F. Chibotaru, W. Wernsdorfer, M. Murugesu, *Angew. Chem. Int. Ed.* **2009**, *48*, 9489–9492; *Angew. Chem.* **2009**, *121*, 9653–9656.
- [9] Y. Peng, A. K. Powell, *Coord. Chem. Rev.* **2021**, *426*, 213490.
- [10] a) S. K. Langley, D. P. Wielechowski, V. Vieru, N. F. Chilton, B. Moubaraki, B. F. Abrahams, L. F. Chibotaru, K. S. Murray, *Angew. Chem. Int. Ed.* **2013**, *52*, 12014–12019; *Angew. Chem.* **2013**, *125*, 12236–12241; b) S. K. Langley, N. F. Chilton, L. Ungur, B. Moubaraki, L. F. Chibotaru, K. S. Murray, *Inorg. Chem.* **2012**, *51*, 11873–11881.
- [11] C. van Wüllen, *J. Phys. Chem. A* **2009**, *113*, 11535–11540.
- [12] A. Dey, J. Acharya, V. Chandrasekhar, *Chem. Asian J.* **2019**, *14*, 4433–4453.
- [13] A. M. Ako, I. J. Hewitt, V. Mereacre, R. Clérac, W. Wernsdorfer, C. E. Anson, A. K. Powell, *Angew. Chem. Int. Ed.* **2006**, *45*, 4926–4929; *Angew. Chem.* **2006**, *118*, 5048–5051.
- [14] F.-S. Guo, B. M. Day, Y.-C. Chen, M.-L. Tong, A. Mansikkamäki, R. A. Layfield, *Science* **2018**, *362*, 1400.
- [15] a) M. Pinsky, D. Avnir, *Inorg. Chem.* **1998**, *37*, 5575–5582; b) S. Alvarez, D. Avnir, M. Llunell, M. Pinsky, *New J. Chem.* **2002**, *26*, 996–1009; c) D. Casanova, J. Cirera, M. Llunell, P. Alemany, D. Avnir, S. Alvarez, *J. Am. Chem. Soc.* **2004**, *126*, 1755–1763; d) S. Alvarez, P. Alemany, D. Casanova, J. Cirera, M. Llunell, D. Avnir, *Coord. Chem. Rev.* **2005**, *249*, 1693–1708.
- [16] a) A. Ruiz-Martínez, D. Casanova, S. Alvarez, *Chem. Eur. J.* **2008**, *14*, 1291–1303; b) D. Casanova, M. Llunell, P. Alemany, S. Alvarez, *Chem. Eur. J.* **2005**, *11*, 1479–1494.
- [17] M. Murugesu, A. Mishra, W. Wernsdorfer, K. A. Abboud, G. Christou, *Polyhedron* **2006**, *25*, 613–625.
- [18] a) V. Mereacre, A. Baniodeh, C. E. Anson, A. K. Powell, *J. Am. Chem. Soc.* **2011**, *133*, 15335–15337; b) A. Baniodeh, Y. Lan, G. Novitchi, V. Mereacre, A. Sukhanov, M. Ferbinteanu, V. Voronkova, C. E. Anson, A. K. Powell, *Dalton Trans.* **2013**, *42*, 8926–8938.
- [19] A. Baniodeh, V. Mereacre, N. Magnani, Y. Lan, J. A. Wolny, V. Schünemann, C. E. Anson, A. K. Powell, *Chem. Commun.* **2013**, *49*, 9666–9668.
- [20] Y. Peng, V. Mereacre, C. E. Anson, A. K. Powell, *Phys. Chem. Chem. Phys.* **2016**, *18*, 21469–21480.
- [21] Y. Peng, V. Mereacre, C. E. Anson, A. K. Powell, *ACS Omega* **2018**, *3*, 6360–6368.
- [22] S. Mukherjee, M. R. Daniels, R. Bagai, K. A. Abboud, G. Christou, C. Lampropoulos, *Polyhedron* **2010**, *29*, 54–65.
- [23] G. Peng, G. E. Kostakis, Y. Lan, A. K. Powell, *Dalton Trans.* **2013**, *42*, 46–49.
- [24] G. Peng, V. Mereacre, G. E. Kostakis, J. A. Wolny, V. Schünemann, A. K. Powell, *Chem. Eur. J.* **2014**, *20*, 12381–12384.
- [25] H. Xiang, V. Mereacre, Y. Lan, T.-B. Lu, C. E. Anson, A. K. Powell, *Chem. Commun.* **2013**, *49*, 7385–7387.
- [26] N. N. Greenwood, *Mössbauer Spectroscopy*, Springer, Netherlands **1971**.
- [27] R. D. Cannon, R. P. White, *Prog. Inorg. Chem.* John Wiley and Sons, Inc., New York, **1988**, pp. 195–298.
- [28] V. Vieru, L. Ungur, V. Cemortan, A. Sukhanov, A. Baniodeh, C. E. Anson, A. K. Powell, V. Voronkova, L. F. Chibotaru, *Chem. Eur. J.* **2018**, *24*, 16652–16661.
- [29] Y. Peng, M. K. Singh, V. Mereacre, C. E. Anson, G. Rajaraman, A. K. Powell, *Chem. Sci.* **2019**, *10*, 5528–5538.
- [30] K. C. Mondal, A. Sundt, Y. Lan, G. E. Kostakis, O. Waldmann, L. Ungur, L. F. Chibotaru, C. E. Anson, A. K. Powell, *Angew. Chem. Int. Ed.* **2012**, *51*, 7550–7554; *Angew. Chem.* **2012**, *124*, 7668–7672.
- [31] K. Kambe, *J. Phys. Soc. Jpn.* **1950**, *5*, 48–51.
- [32] H. Xiang, V. Mereacre, Y. H. Lan, T. B. Lu, C. E. Anson, A. K. Powell, *Chem. Commun.* **2013**, *49*, 7385–7387.
- [33] D. Schray, G. Abbas, Y. Lan, V. Mereacre, A. Sundt, J. Dreiser, O. Waldmann, G. E. Kostakis, C. E. Anson, A. K. Powell, *Angew. Chem. Int. Ed.* **2010**, *49*, 5185–5188; *Angew. Chem.* **2010**, *122*, 5312–5315.
- [34] A. Baniodeh, I. J. Hewitt, V. Mereacre, Y. Lan, G. Novitchi, C. E. Anson, A. K. Powell, *Dalton Trans.* **2011**, *40*, 4080–4086.
- [35] A. Baniodeh, N. Magnani, Y. H. Lan, G. Buth, C. E. Anson, J. Richter, M. Affronte, J. Schnack, A. K. Powell, *npj Quantum Mater.* **2018**, *3*, 6.
- [36] A. Baniodeh, Y. Liang, C. E. Anson, N. Magnani, A. K. Powell, A.-N. Unterreiner, S. Seyfferle, M. Slota, M. Dressel, L. Bogani, K. Goß, *Adv. Funct. Mater.* **2014**, *24*, 6280–6290.
- [37] H. Kaemmerer, A. Baniodeh, Y. Peng, E. Moreno-Pineda, M. Schulze, C. E. Anson, W. Wernsdorfer, J. Schnack, A. K. Powell, *J. Am. Chem. Soc.* **2020**, *142*, 14838–14842.

Manuscript received: August 13, 2021

Accepted manuscript online: September 28, 2021

Version of record online: ■■■, ■■■■

## REVIEW



The well-known oxo-centred Fe triangle is used to access the vast majority of  $[\text{Fe}^{\text{III}}_2\text{Ln}_2(\mu_3\text{-OR})_2\text{L}_2(\text{O}_2\text{CR})_6]$  butterflies, since it provides a di-iron central body unit and carboxylate bridges to the wingtips, which are occupied by supplied Ln ions. The remaining coordination sites of the

lanthanide are occupied by a multi-dentate ligand, which can also provide further bridging. This system provides a useful testbed for exploring multiple variations, for example changing the Ln, the bridging carboxylate and the nature of the chelating ligand.

*Dr. Y. Peng\*, H. Kaemmerer, Prof. A. K. Powell\**

1 – 24

**From the  $\{\text{Fe}^{\text{III}}_2\text{Ln}_2\}$  Butterfly's Perspective: the Magnetic Benefits and Challenges of Cooperativity within 3d–4f Based Coordination Clusters**

